PLASTIC DEFORMATION OF HIGH-PURITY IRON SINGLE CRYSTALS

Aono, Yasuhisa
Research Institute for Applied Mechanics, Kyushu University : Research Associate

Kuramoto, Eiichi
Research Institute for Applied Mechanics, Kyushu University : Associate Professor

Kitajima, Kazunori
Research Institute for Applied Mechanics, Kyushu University : Professor

https://doi.org/10.5109/6779636

出版情報：Reports of Research Institute for Applied Mechanics. 29 (92), pp.127-193, 1981-09.
九州大学応用力学研究所
バージョン：
権利関係：

Reports of Research Institute for Applied Mechanics
Vol. XXIX, No. 92, 1981

PLASTIC DEFORMATION OF HIGH-PURITY IRON SINGLE CRYSTALS

By Yasuhisa AONO*, Eiichi KURAMOTO**
and Kazunori KITAJIMA***

High-purity iron single crystals of various sizes were strained in tension at very low temperatures to investigate the intrinsic plastic behaviours as a function of crystal orientation and temperature. The ability of slip deformation at 4.2 K strongly depended on the specimen size and the specimens of a smaller size (0.2 mm in diameter) could be deformed by slip at any orientation. Several characteristics of slip in iron were obtained from tensile tests in a wide temperature range 0.7 to 400 K, namely, i) the τ_y—χ relation of asymmetric concave type (orientation dependence of yield stress), ii) $(\bar{1}01)$ slip plane for gliding of primary dislocations at 4.2 K, iii) a hump on τ_y—T curve (temperature dependence of yield stress), which corresponds to a peak on A^*—τ_y curve (stress dependence of activation area). The results were consistently interpreted from a standpoint of the intrinsinc lattice friction (Peierls mechanism) to a screw dislocation motion and the nature of the core structure of it.

Key words: Iron, High-purity, Single crystal, Plastic deformation, Peierls mechanism, Screw dislocation

1. Introduction

On the tensile properties of iron at very low temperatures, many studies have been made since the early investigation by Allen et al.[1]. As a well-known fact, twinning and cleavage fracture generally occur at low temperatures below 77 K. The investigation of slip deformation is, therefore, interrupted by twinning since cleavage fracture has been also known to be caused by twinning. Thus lack of data of slip deformation at very low temperatures has so far become a main reason why the fundamental aspects of plastic deformation in iron had not been resolved

* Research Associate, Research Institute for Applied Mechanics, Kyushu University
** Associate Professor, Research Institute for Applied Mechanics, Kyushu University
*** Professor, Research Institute for Applied Mechanics, Kyushu University

yet in spite of many investigations. Namely, the fundamental characteristics such as yield stress for slip at a certain temperature, fundamental slip plane and comprehensive explanation of deformation mechanism (for the whole temperature range), can not be made clear unless the experiment at very low temperatures is performed.

If a critical stress essentially exists in twin deformation, it is impossible to investigate characteristics of slip in the range of higher stress than it. Recently, however, successes[2)~4)] in slip deformation at liquid helium temperature have been reported in BCC transition metals; for iron, Conte et al. on iron whisker[2)], Sato and Meshii on single crystal plates[3)] and Matsui et al. on polycrystals of coarse grain (bamboo type)[4)]. These results are important in a sense that the critical shear stress in twin deformation is higher than that in slip deformation. These studies, however, have not been developed to systematic studies on plastic deformation in a single crystal because they were fragmental reports.

Many investigators have so far made much effort to produce a high-purity specimen from a point of view that the difficulty in slip deformation is due to the influence of impurities in a specimen. Although such an effort is of course indispensable to fundamental behaviour of plasticcity, these investigations have not been succeeded yet with regard to the subject mentioned above. An alternative method which enables slip deformation at very low temperatures is to give a specimen pre-strain at a higher temperature. A specimen, however, can not be deformed by slip at 4.2 K, only by means of this method. Plastic deformation at very low temperatures is generally considered to occur in competition between slip and twinning. The development from twinning to cleavage fracture will need the growth of twins with a adequate size even though the embryos of twins are nucleated in a specimens. This process may be, therefore, closely concerned with the specimen size.

On the other hand, on studies for examining fundamental characteristics or mechanism of slip deformation in iron many studies[2)8)~16)] have been made since the early investigation by Basinski and Christian[5)] and Conrad and Scheock[6)] in the year 1960, over the 1960's to 1970's. The experimental results showed the strong temperature dependence of yield stress below room temperature, which being contrary to FCC metals. Two opinions sharply divided, however, have been offered to the cause of temperature dependence. Stein, Low and Seybolt[10)] and Fleischer[17)] have maintained that it is due to locking of dislocations by interstitial impurities of a very small amount. On the other hand, Basinski and Christian and Conrad and Scheock have offered the opinion of the lattice friction of a dislocation itself. After that, the latter have been experimentally supported as the technique of the purification of a specimen have been advanced. Hirsch[18)] and H. Suzuki[19)] have supported theoretically the latter from a point of view of high Peierls stress of a screw

dislocation due to characteristic of BCC structure. Moreover, Vitek[20] and Takeuchi et al.[21)~25)] have given strong support to this opinion from calculation of the core structure and the motion of a screw dislocation in a model crystal using a computer.

Alternatively, there is the anisotropy of slip as an important problem among characteristics of slip deformation. Namely, slip plane have not been generally determined precisely, in comparison with FCC metals because slip lines in BCC metals have been well-known to be wavy. Also, the average slip plane does not obey Schmid law and is almost crystalographic plane at low temperatures. It has been pointed out that the yield stress and silp systems are different for either tension or compression in pure metals and alloys such as Fe[26)], Mo[27)], W[28)], Ta[29)] and Fe–Si alloy[30)]. This anisotropy of slip in BCC metals have been explained by the nature of the core struture of a screw dislocation[22)~25)], but the mechanism of the anisotropy will be finally made clear only by the experiment at very low temperatures.

Recently, such an interesting subject has experimentally revealed in slip deformation that the rate eqution of classical Arrhenius type is not established at very low temperatures in FCC and BCC metals and ionic crystals. The physical concept which leads theoretically to the rate equation is the thermally activated motion of dislocations over a potential barrier. Deviation from this rate equation at very low temperatures, however, have been reported and the discussion is based on: (1) a quantum mechanical tunnelling effect which aids a dislocation to overcome the potential barrier[31)~34)]; (2) a quantum effect on the vibrational mode of the dislocation due to discrete energy levels and to the zero-point vibration[35)~38)]; (3) a dynamical effect of dislocation motion caused by the high velocity of the dislocation[39)~40)]. The last effect is not operative in BCC metals in which the deformation is governed by the Peierls mechanism. Also, the experiments at very low temperatures are needed for making this phenomenon clear.

The present study is to resolve various subjects which have been still remained in plastic deformation in iron as mentioned above. Therefore, the ability of slip deformation at very low temperatures was examined as first subject of study, mainly, from a point of view of the effect of the specimen size and then the fundamental characteristics of deformation in iron were systematically investigated for comprehensively explaining the mechanism of slip deformation.

2. Experimental procedure

2.1. Materials and specimen prepalation

2.1.1. High-purity iron

Two kinds of pure iron were used in this investigation, i.e. the re-

electrolytic iron supplied by the Iron and Steel Institute of Japan and a pure iron of Material Research Corpolation (MARZ-grade). Their starting materials are reported to contain metallic impurities of about 100 wppm and less than 10 wppm as listed in Table 1, being marked as RE and MRC, respectively. For eliminating gas impurities in these starting materials, carbon, nitrogen and oxygen atoms, first, the rods of these materials were chemically polished in a 20 : 1 solution of H_2O_2 and HF and then zone-refined at a refining speed of 1 mm/min in a flowing hydrogen gas, which was palladium-purified: one pass in wet hydrogen and five passes in dry hydrogen using a HF heating-type floating-zone melting apparatus, and in vacuum of 10^{-4} Pa (in melting state) using an electron-beam floating-zone apparatus.

The zone-refined rods of 10 mm in diameter shown in Fig. 1 were cold-rolled into rods of 2 mm in square. The intermediate annealing was

Table 1. The residual impurities in the as-received materials.

i) Re-electrolytic iron (wppm)

C	N	O	Si	Mn	P	S	Cu	Ni	Co
40	20	13	40	43	27	45	32	41	78

ii) MRC iron (wppm)

C	N	O	Cr	Ti	Zn	S	K	Na
12	10	30	1	1	2	3	1	1

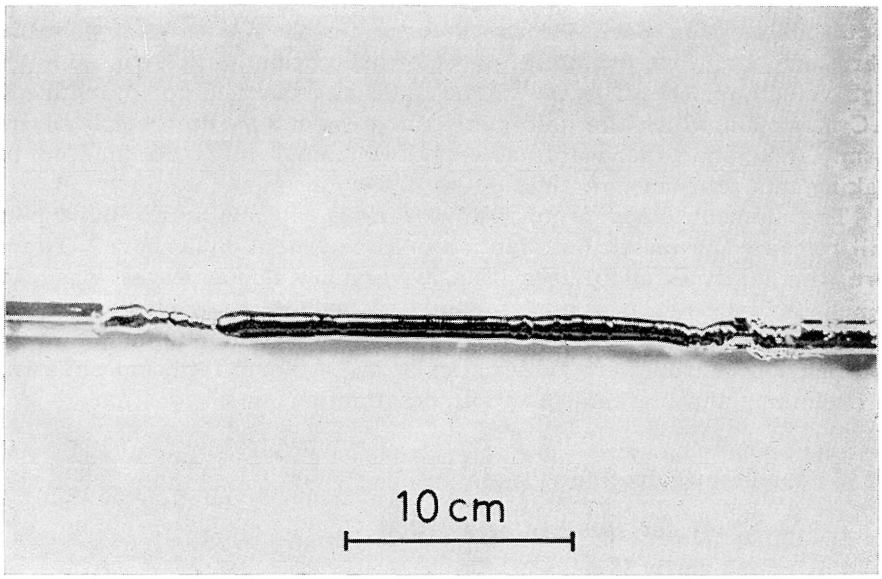

Fig. 1 A sample of MRC iron rod zone-refined in hydrogen gas and vacuum.

performed at 600°C in a flowing hydrogen gas for rods of 8, 4 and 2 mm in square, respectively. After metallurgically and then chemically polishing, the rods of 2 mm in square were finally drawn to wires of 0.3, 0.55 and 1 mm in diameter for RE and 0.3, 0.4 and 0.6 mm in diameter for MRC. Moreover, in order to obtain the sheet specimens with the cross section $0.25 \times 2\text{–}5\,mm^2$ the wires of MRC were cold-rolled, cut into the width of 0.4–1.3 mm, and then metallurgically and chemically polished to smooth the sides of sheets.

Single crystals were grown by the strain-annealing method. Before using this method, however, nitrogen was doped into the wires of 0.3 mm in diameter and all other MRC specimens at 600°C in a flowing dry hydrogen gas which passed through liquid ammonia cooled at 200 K because it was very difficult to produce single crystals of a small size and high-purity by this method without doping. For removing doped nitrogen and residual gas impurities, single crystals chemically pollished were annealed under the condition of hydrogen treatment as shown in Table 2. The wires and sheets of single crystals thus hydrogen-treated were chemically polished to remove the surface layer contaminated by silicon in quarz tube during annealing[42)~43)]. The residual resistivity ratio, RRR_H (the ratio of the electrical resistivity at room temperature to that at helium temperature under the longitudinal magnetic field of 800 Oe) of specimens was about 400 for RE and 3500–4400 for MRC. The small ratio of RE will be probably due to residual metallic impurities. On the other hand, gas impurities is considered to be almost eliminated by melting and finally annealing in hydrogen gas for both RE and MRC. For example, Kitajima[44)] has assumed that the concentration of oxygen was below the limit of analysis, 2 wppm and that the solute carbon was below the limit of the measurement by internal friction method, 0.1 wppm. Takagi and Kimura[42)], whose iron has been purified by zone-melting in ultra-high vacuum of about 10^{-6} Pa and then the same hydrogen treatment as the present work, have also reported that the total concentration of carbon having precipitated and solved in their iron with RRR_H of 3600 was about 0.2 wppm.

Table 2. Condition of hydrogen-treatment

specimen	size	wet H_2	dry H_2
RE	0.2	20 hrs at 800°C	20 hrs at 600°C
	0.5	50	50
	1.0	110	50
MRC	0.2	12	6
	0.4	20	20
	0.6	35	20
S-MRC	0.4	20	12
	1.2	20	12

The final shapes of the specimens of 20 mm long with the guage length of 10 mm were as follows: wires of 0.2, 0.5 and 0.97 mm in diameter for RE (marked as RE (0.2), RE (0.5) and RE (1), respectively), wires of 0.2, 0.37 and 0.57 mm in diameter for MRC (marked as MRC (0.2), MRC (0.4) and MRC (0.6)) and sheets of 0.35 and 1.2 mm in width with the thickness of 1.5–0.2 mm (marked as S-MRC (0.4) and S-MRC (1.2)).

The orientation of a specimen was represented by parameters shown in Fig. 2, where λ is the angle between the tensile axis and the primary slip direction [111] in BCC metals and χ the angle between the maximum shear stress plane, M containing the direction [111] and ($\bar{1}01$) plane. Also ψ in the figure is the angle between the observed slip plane, O and ($\bar{1}01$) plane, and the orientation dependence of active slip plane is denoted by the $\psi-\chi$ relation. A and B are orientations of specimens for the measurement of the temperature dependence of yield stress and the activation parameters in each orienation.

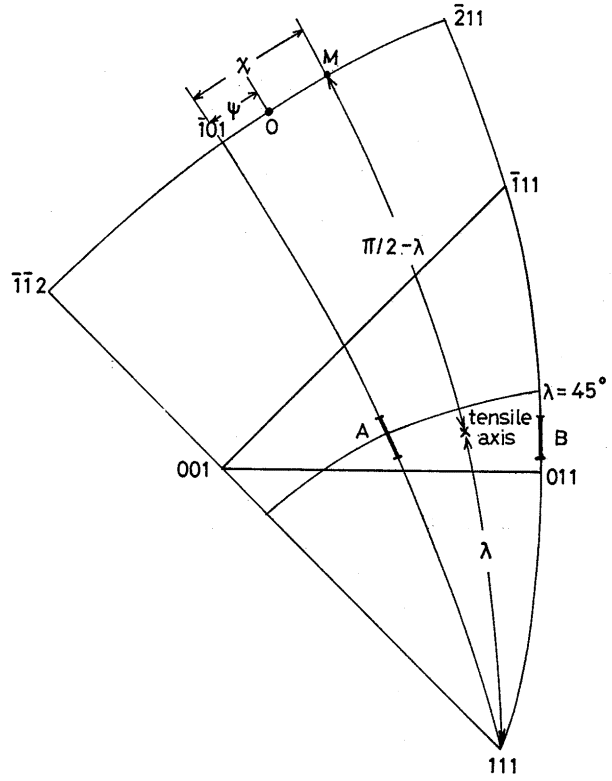

Fig. 2 Stereographic projection for the orientation of a tensile specimen.

2.1.2. Carburization and quenching

Among single crystals of MRC, those of oreintation A were chosen for producing Fe-C alloy specimens. The wire specimens of 0.2 mm in diameter and 70 mm long were carburized at 700°C for 30 min in a flowing dry hydrogen gas which passed through n-heptane cooled at 200 K and then cooled down from the furnace to room temperature. To disperse carbon atoms uniformly in the specimens, the quenching was then performed: the carburized specimens were heated in a purified argon atmosphere at 700°C for 30 min and then quenched into the mixture of ice and water. The specimens of Fe-C alloy thus produced were quickly held in liquid nitrogen to prevent carbon atoms from migrating and forming clusers. Moreover, these specimens were cut into 20 mm long in liquid nitrogen before tensile test. The carbon concentration in carburized-quenched specimens was estimated as 150 appm by measuring the change in the electrical resistivity at 77 K due to the introduce of carbon atoms and using the value of 6.0 $\mu\Omega$cm/at%C by Wagenblast and Arajs[45].

2.2. Tensile test and cryostat

Tensile tests were preformed at a normal strain-rate of 1.7×10^{-4} sec^{-1} in a wide temperature range 0.7 to 400 K. Test temperatures were controlled within 1 % of a given temperature using helium cryostats and liquid baths listed in Table 3. Two kinds of helium cryostat, ^{3}He and ^{4}He cryostats were used for obtaining very low temperatures below 77 K. Tensile test below 4.2 K were performed in a ^{3}He cryostat connected to an Instron testing machine in Institute for Solid state physics, University of Tokyo. Figs. 3 and 4 show the schematic illustration of the whole apparatus including ^{3}He cryostat and the tensile testing machine, and the enlarged cross sectional view of the chamber, repectively. ^{3}He gas of 99.9 % quality was liquidized in the ^{3}He chamber temperature of which was about 1.6 K. ^{3}He liquid of about 12 cc was obtained within 10 min in the ^{3}He chamber, which is seperated from liquid ^{4}He by the vacuum space of about 2.7×10^{-3} Pa. A pulling rod of 2 mm in diameter runs into the ^{3}He camber through bellows which enable the frictionless pulling test. Then the temperature of liquid ^{3}He was lowered usually to 0.7 K, occasi-

Table 3. Controlled temperature baths for tensile tests

temperature (K)	bath
$0.7 \leqq T < 4.2$	pumped liquid ^{3}He and ^{3}He gas
4.2	liquid ^{4}He
$4.2 < T < 77$	^{4}He gas or ^{3}He gas
77	liquid N_2
90	liquid O_2
$90 < T < 200$	liquid propane
$200 \leqq T \leqq 300$	alcohol
$300 > T$	silicon oil

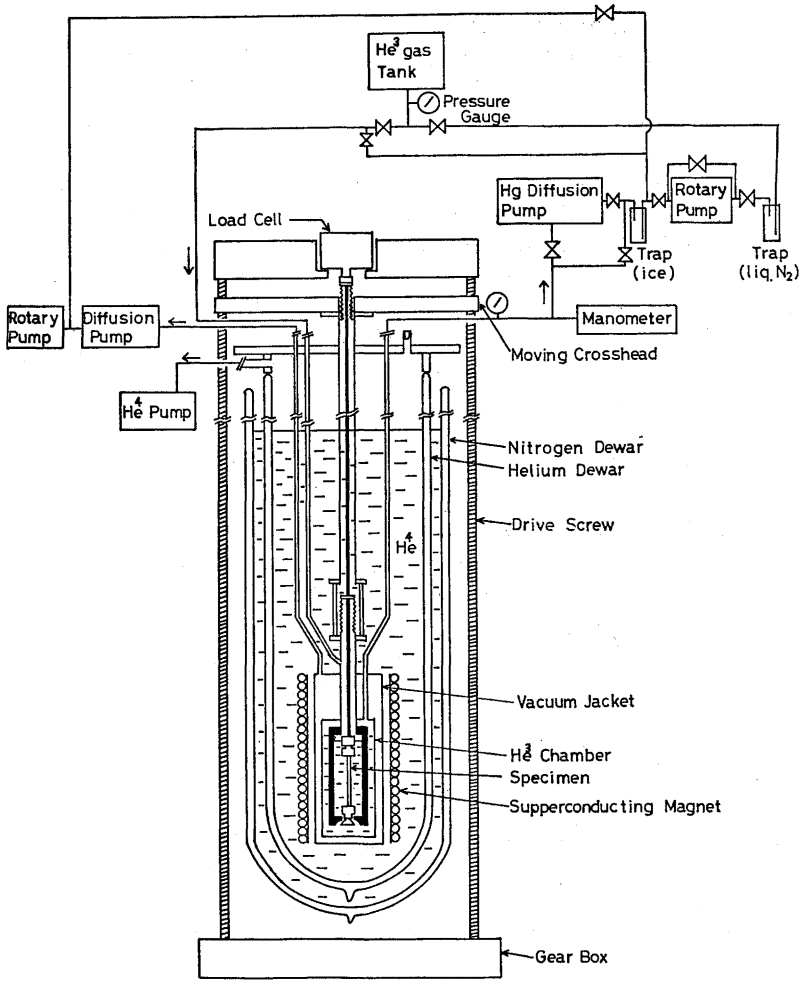

Fig. 3 Schematic illustration of the tensile testing apparatus connected to the ^{3}He cryostat and its circulation system of ^{3}He.

onally to 0.5 K, by pumping with the mercury and the rotary pump of gas tight type. Temperature was measured by germanium thermometer. A wire specimen of 0.2 mm in diameter was soldered to a grip and set in a tensile jig in the ^{3}He specimen chamber: one end of the specimen was put into and soldered to a small steel ball which was free from the tensile jig before straining. Specimens were pre-strained to a small amount of plastic strain, 0.5 % at 77 K and then strained in lquid ^{3}He and in cooled ^{3}He gas for tests below and above 3.2 K, respectively. The pre-straining seemed to increase the elongation at helium temperature, although specimens without pre-straining did not exhibit twinning at

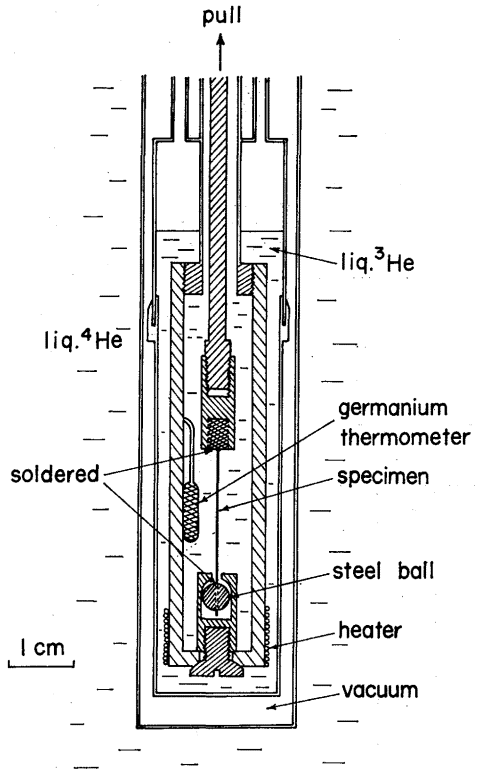

Fig. 4 Cross sectional view of a liquid ^{3}He cryostat used in the tensile test.

helium temperature as understood from later results. To measure the temperature dependence of yield stress a specimen was repeatedly tested, the amount of strain at each temperature being less than 0.3 %. A small amount of stress increase due to work hardening was subtracted from the value of the flow stress at each test and the change of Schmid factor and cross section caused by straining were also corrected.

On the other hand, tensile test in the temperature range 4.2 to 77 K were performed mainly in a ^{4}He cryostat as shown in Fig. 5, although a ^{3}He cryostat was also used partly. The setting of a chucked specimen to the tensile jig was carried out as explained below: the chucked specimen, which was suspended with a wire, was put down through the hole in the flange, placed on the guide fixed to the upper pedestal and set onto the pedestal by operating the tongs which were introduced into glass dewar. The chucks were tied up with a thin wire so that they could be quickly withdrawn out of the dewar after testing. Many specimens could be tested with one charge of liquid helium using this cryo-

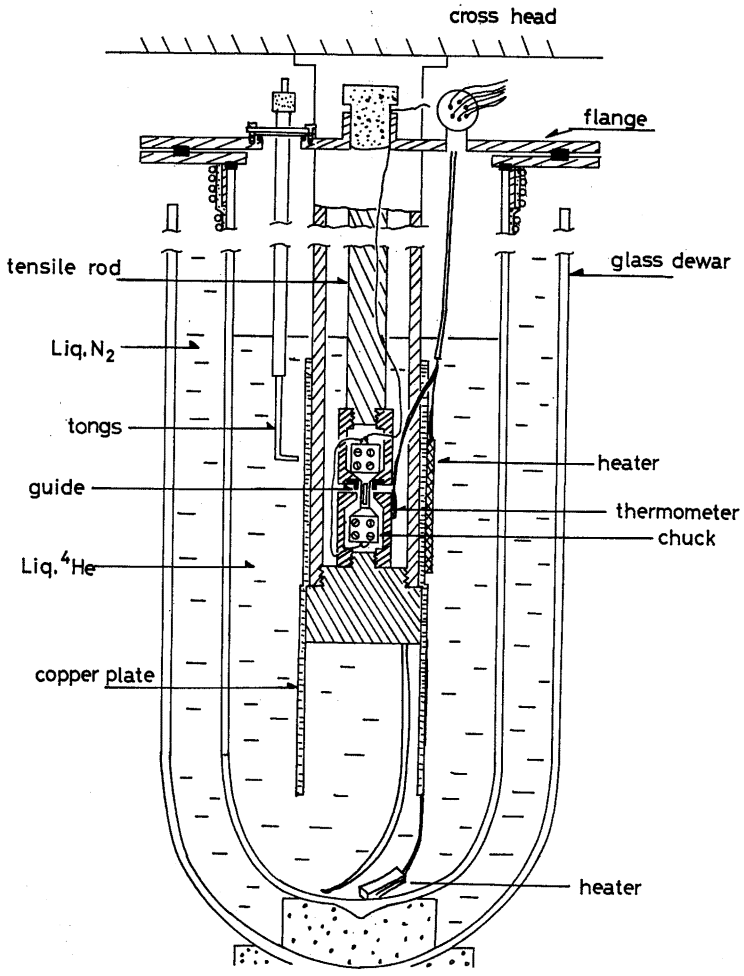

Fig. 5 Cross sectional view of a liquid ^{4}He cryostat used in the tensile test.

stat. Also, for tests at temperatures above 4.2 K the pedestals were surrounded with a chamber made of copper tube and a temperature was controlled using a heater fixed on it. Temperature was measured by thermocouple of Chromel-Au-0.07 at%Fe.

In order to prevent mishandling bend of specimens, all thin specimens were guarded by a pipe guide attached to a chuck and fixed to the chucks in liquid nitrogen. Some of specimens were soldered to end pieces to avoid straining due to chucking. Fig. 6 shows the schematical illustration of chucks.

The strain-rate sensitivity of yield stress and flow stress was mea-

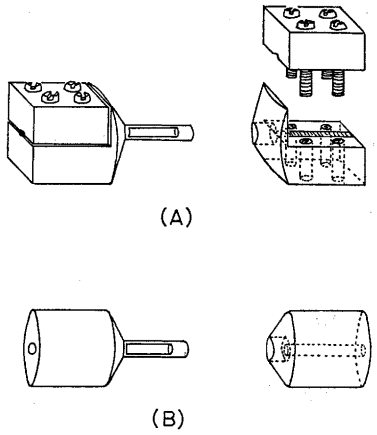

Fig. 6 Chucks which fix a rod specimen with the screw (A) and the solder (B). The weight of a small chuck is two grams.

sured by stress relaxation test at temperatures above 4.2 K. However, strain-rate change test was also carried out by increasing the strain-rate by a factor ten instead of stress relaxation at temperatures below 4.2 K and around helium temperature because the amount of stress relaxation was very small at very low temperatures.

2.3. Observation by optical and electron microscope

Twin and slip traces on the surface of a deformed specimen were observed using an optical microscope of Olympus N-TR type with Nomarski interference contrast. The slip plane was determined from the operation as follows: a deformed sheet specimen was first X-ray photographed to determine the new axial orientation and the surface (top and side) orientations, the angle between the slip trace on the surface and the tensile axis was obtained from the photographs of slip traces and analysis was completed by plotting these informations together with the X-ray results on a streogram and rotating the poles into the standard projection. The slip trace analysis was accurate to $<2°$ for perfectly crystalographic slip line, but, where the slip traces were wavy, the precision deteriorated accordingly and therefore the direction of slip line was avereged.

The twin and dislocation structure in a deformed specimen was observed using a high-voltage electron microscope JEM-1000 in Kyushu University operating at 1250 V. After deformation, the gauge length section of a sheet specimen was cut with an acid saw into three pieces of about 3 mm long and each of them was chemically polished to a thickness of 0.1 mm. Electron transparent foils were prepared under the electrolytic condition of 45 mA and 14 V. The electrolyte used was a solution of

accetic acid (450 cc), perchrolic acid (50 cc) and methanol (50 cc).

3. Experimental results

Experiments were first made for examing the ability of slip deformation in our iron single crystals at very low temperatures, and then for obtaining various characteristics of slip in high-purity iron single crystals.

3.1. Deformation-mode at very low temeratures

3.1.1. Stress-strain curves

i) Stress-strain curves for RE iron

The stress-strain curves for wire specimens of RE in the temperature range 64 to 200 K are shown in Fig. 7. In the RE(1) specimen twinning occurred either before or after macroyielding by slip at temperatures below 90 K, though down to 64 K a few specimens were able to be deformed by slip only at orientations of $\chi \geqq 0°$. Generally, as temperature was lowered, the number of twin and the amount of stress drop due to twinning increased and the stress level of twin nucleation was lowered. The RE(0.5) and RE(0.2) specimens, however, were deformed by slip at all orientations without twinning.

At 4.2 K all the RE(1) specimens were fractured by cleavage at a

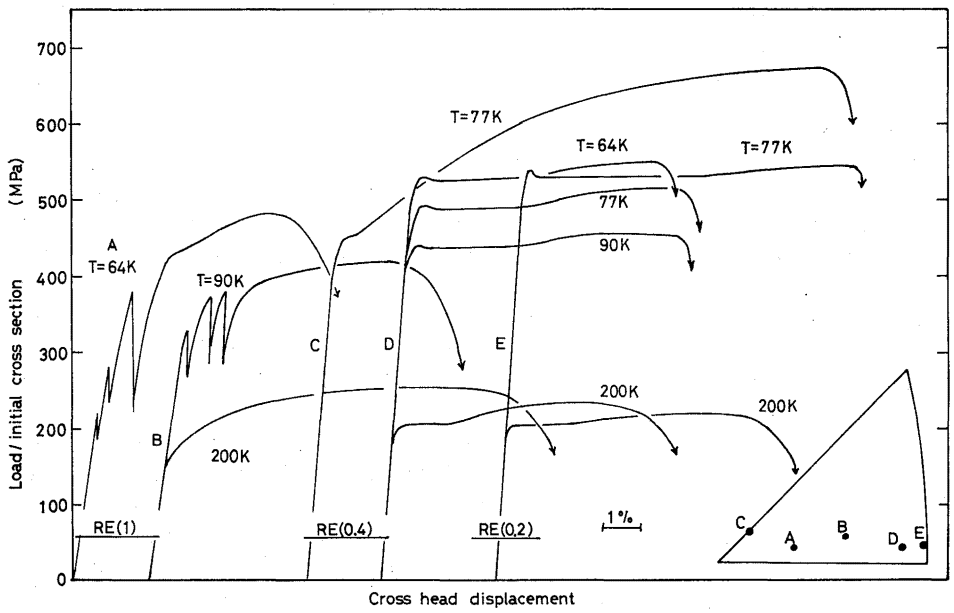

Fig. 7 Stress-strain curves for RE iron in the temperature range 64 to 200 K.

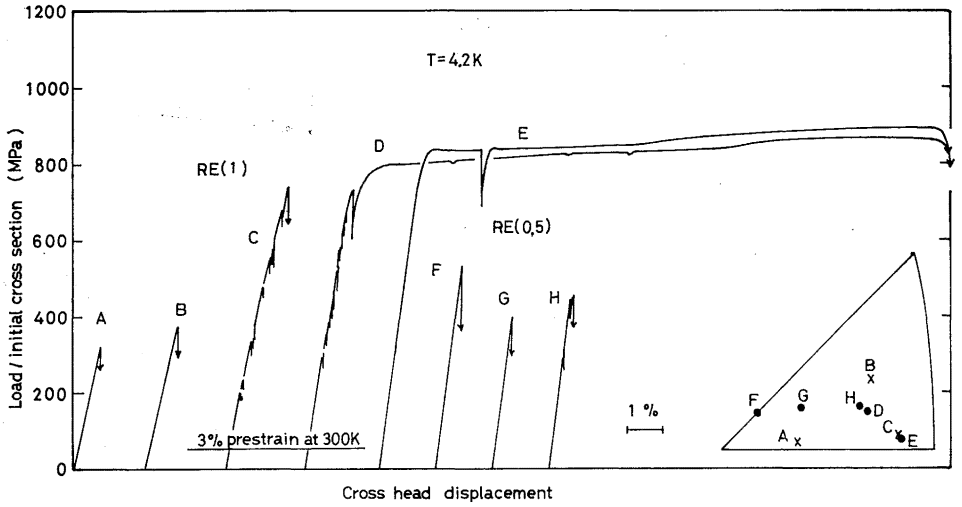

Fig. 8 Stress-strain curves for RE(1) (×) and RE(0.5) (•) at 4.2 K.

low stress level as illustrated in Fig. 8. Pre-straining at room temperature increased fracture stress, but caused microtwins in the proportional region. Some of RE(0.5) specimens, however, showed yielding by slip without twinning, and were deformed up to about 15 % strain, then slipped off showing chisel edge apparance, though many specimens were fractured by cleavage either with or without twin bursts just before or after yielding at a high stress level. The pre-straining of 0.3–3 % at room temperature was effective in suppression of twin bursts and cleavage fracture, and made most of the specimens ductile at 4.2 K, through there appeared the microtwins in the proportional region as well as the RE(1) specimens as illustrated in the same figure.

When the diameter was further reduced to 0.2 mm, most of the specimens could be deformed by slip at 4.2 K without pre-straining, though a few twins were sometimes formed as seen in Fig. 9. Twinning generally occurred at a higher stress level in comparision with the RE specimens with larger diameters, namely, just near yielding at orientations of $\chi < 0°$ and in the region of flow stress at those of $\chi \geqq 0°$. These twins, however, were completely suppressed by slightly pre-straining of 0.5–1 % at room temperature.

By way of a trial, the RE(0.5) specimens with the effective gauge length of 7.5, 10, 20, 30 and 40 mm were deformed at 4.2 K. The result was that the behaviour of deformation was independent of the gauge length, namely, deformation-mode seems to depend on only the specimen size.

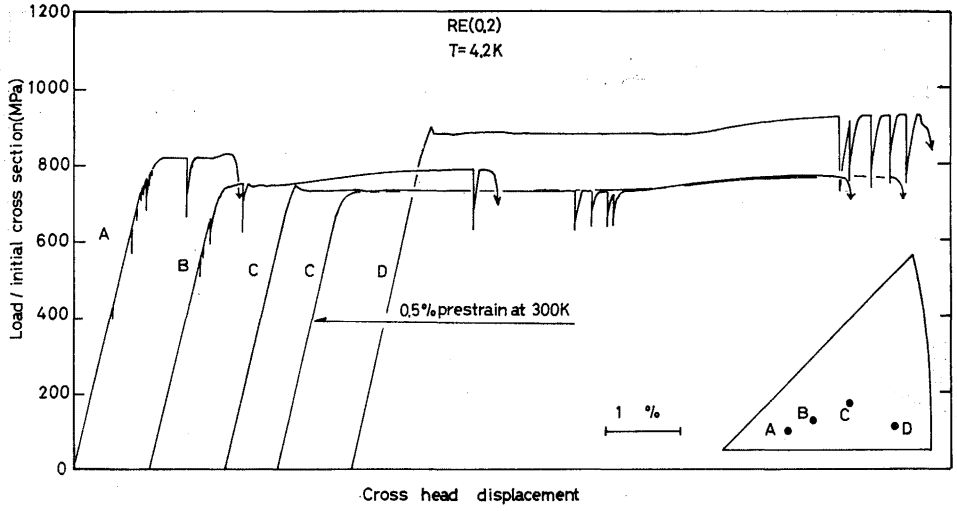

Fig. 9 Stress-atrain curves for RE(0.2) at 4.2 K.

ii) Stress-strain curves for MRC iron

The stress-strain curves for MRC specimens with the diameters of 0.2–0.6 mm at temperatures above 64 K are shown in Fig. 10. In this temperature range all the MRC specimens were deformed only by slip. At 4.2 K, however, the effect of specimen size became remarkable as shown in Figs. 11–13. For the MRC(0.6) specimens, 70 % of those tested were fractured by cleavage with twinning at a low stress level (orientations A and B in Fig. 11) and those which even yielded by slip formed twin bursts in the region of flow stress (orientations C and D). The prestrain of more than 1 % had a good effect on the ability of slip deformation for all the specimens without forming many microtwins before micro-yielding.

For the MRC(0.4) specimens in Fig. 12, half of those were deformed by slip with twinning and a few specimens did only by slip up to about 7 % strain. Pre-straining enhanced the suppression of twinning and the elongation by slip.

When the diameter of a specimen was further reduced to 0.2 mm, most of the specimens gave the stress-strain curves of slip only, with good reproducibility as shown in Fig. 13. It is generally recognized that the wire specimens of MRC iron have more ability of slip deformation than those of RE iron with the same size.

On the other hand, the sheet specimens of MRC iron were tested at 4.2 and 77 K. At 77 K all the specimens were deformed by slip and gave the same elongation as the MRC(0.4) specimens. At 4.2 K only a few specimens were able to be deformed by slip as shown as shown in Fig.

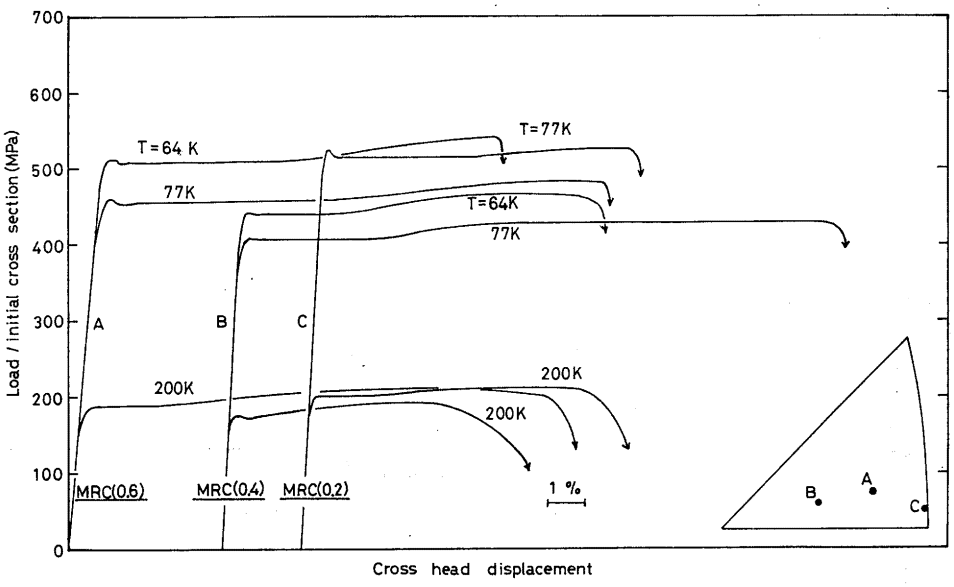

Fig. 10 Stress-strain curves for MRC iron in the temperature range 64 to 200 K.

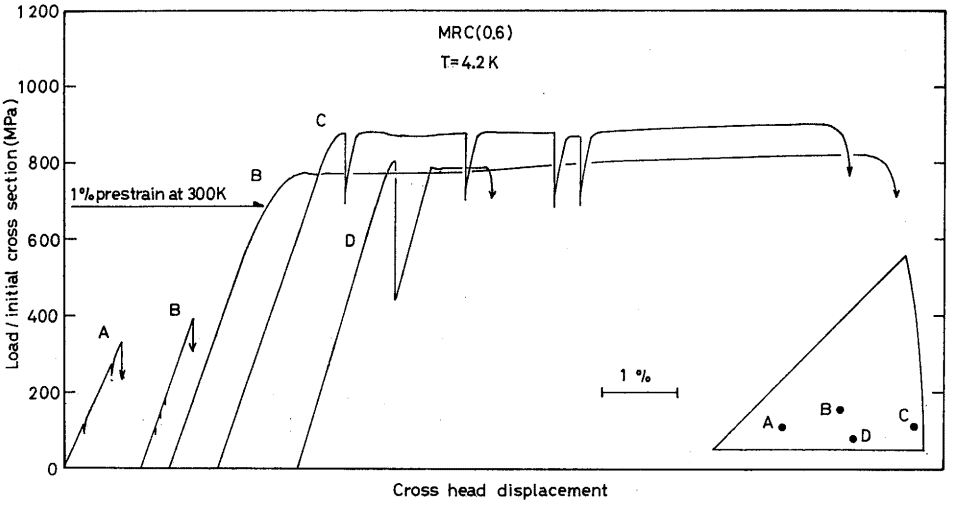

Fig. 11 Stress-strain curves for MRC(0.6) at 4.2 K.

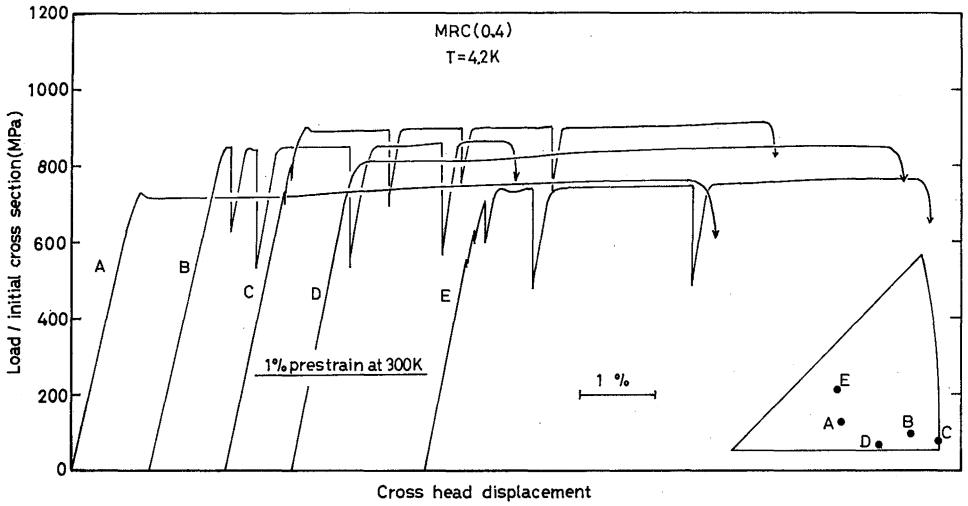

Fig. 12 Stress-strain curves for MRC(0.4) at 4.2 K.

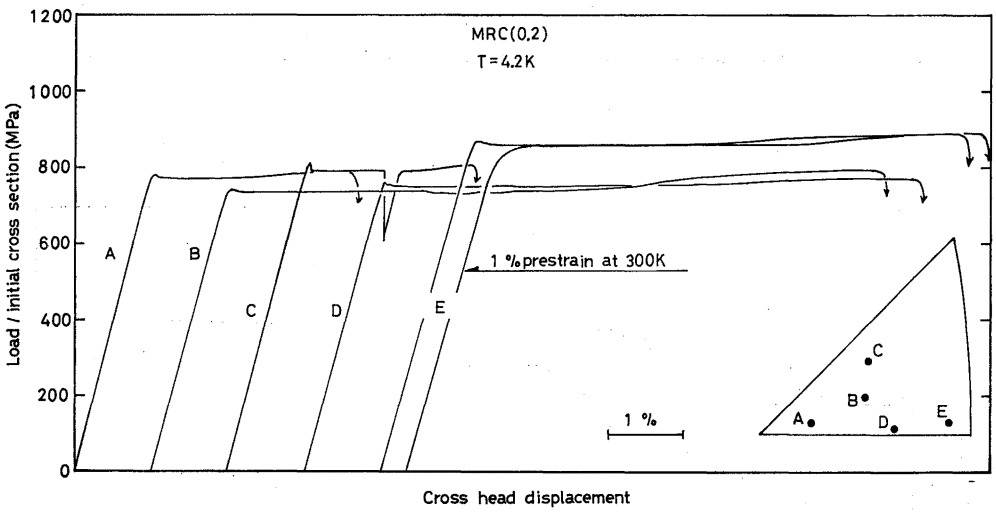

Fig. 13 Stress-strain curves for MRC(0.2) at 4.2 K.

14 and many specimens were accompanied with twinning or were fractured by cleavage at a low stress level. For the specimens with larger width, particularly, slip deformation was quite difficult and, for example, the specimens with the width of 1.2 mm were fractured by cleavage after twinning or only by cleavage.

Fig. 15 shows the stress-strain curves for the specimens pre-strained by 0.5 % at 77 and 300 K. Pre-straining enhanced the ability of slip de-

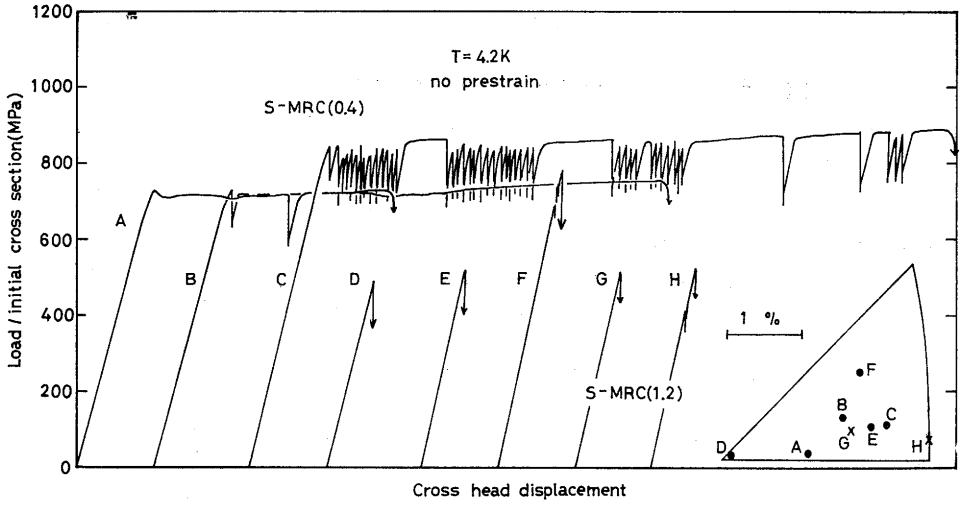

Fig. 14 Stress strain curves for S-MRC(0.4) (•) and S-MRC(1.2) (×) with no pre-strain at 4.2 K.

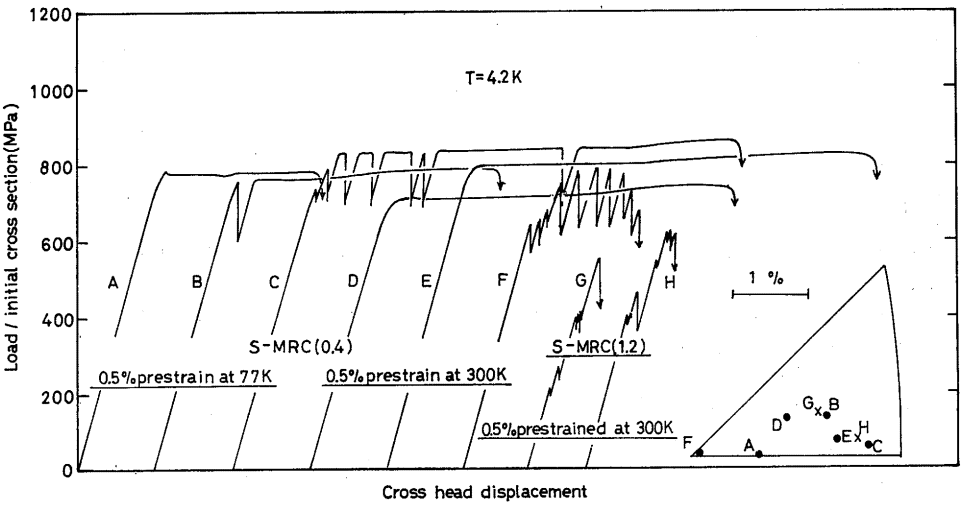

Fig. 15 Stress-srain curves at 4.2 K for S-MRC(0.4) (•) and S-MRC(1.2) (×) pre-strained at 77 and 300 K.

formation at 4.2 K only for the S-MRC(0.4) specimens. The pre-straining at 77 K elevated the level of twin-nucleated stress, but easily caused twin bursts and gave slightly smaller elongation than that at 300 K. The S-MRC(1.2) specimens, however, were impossible to be deformed by slip, even with pre-strain of 0.5 %. The realization of slip deformation need-

ed the pre-strain of more than 1 % for S-MRC(0.4) and more than 3 % for S-MRC(1.2).

iii) Stress-strain curves for impure MRC iron

In order to examin the influence of interstitial impurities, i.e. carbon atoms, their clusters and precipitates on the nucleation of twins, the wire specimens of MRC iron with $RRR_H \simeq 400$, which were not fully hydrogen-treated to eliminate interstitial impurities, were tested at 4.2 K. Fig. 16 shows the typical stress-strain curves of them. The MRC(0.4) specimens were fractured by cleavage without any slip. The MRC(0.2) specimens of a smaller size, however, were not fractured by cleavage, but yielded by slip forming many microtwins in the proportional region and were deformed by slip and twinning alternately in the region of flow stress. Pre-straining at room temperature suppressed the nucleation of twins. Also the carburized-quenched MRC(0.2) specimens, in which carbon atoms were considered to be fully solved, were deformed by slip with a few twims at 4.2 K, details of which will be mentioned in a later section.

3.1.2. Orientation dependence of deformation-mode at 4.2 K

Characteristic features of stress-strain curves for the specimens with typical orientations were reported in a previous section. In this section the orientation dependence of deformation-mode at 4.2 K was summarized from the experimental results obtained. Namely, the deformation-mode was denoted in Fig. 17 from various points of view of the effects of specimen size and shape and pre-straining on deformation for RE and MRC irons, classifying each step as follows: (1) slip, (2) slip with a few twins, (3) slip with many twins, (4) twinning, (5) twinning and cleavage and (6) cleavage. Also Fig. 18 shows the summary of the results in Fig. 17.

i) for the RE(1) and S-MRC(1.2) specimens, slip deformation is difficult at any orientation and the modes are denoted by (5) and (6). Pre-straining at room temperature slightly improves the mode into (3) and (4) only for the MRC(1.2) specimens with orientations of $\chi > 0°$.

ii) for the RE(0.5), MRC(0.6) and S-MRC(0.4) specimens, the modes are (4)-(6) at orientations of $\chi < -10°$ and $\lambda > 50°$. At orientations of $\chi > -10°$ and $\lambda < 50°$, it generally tends to be (1)-(3), but is (4) at those of higher values of χ and λ and approaches (1) at those with the value of $-10° < \chi < 15°$. By pre-straining at 77 K and room temperature, the mode is pointed to (1) in comparison with unstraining.

iii) the MRC(0.4) specimens denotes the mode of (6), (1)-(3) and especially (1) at orientations of $\chi < 0°$, $\chi \geqq 0°$ and $\lambda < 50°$, and $0° < \chi \leqq 15°$, respectively.

iv) the RE(0.2) and MRC(0.2) specimens of the smallest size denotes almost the same mode at any orientation, details of which being that

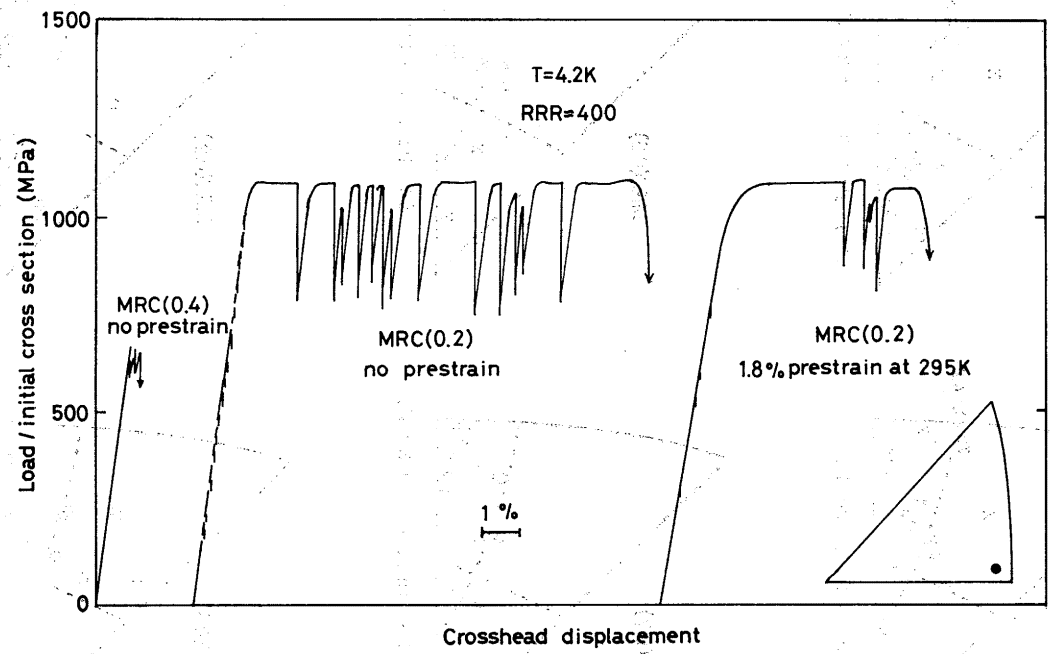

Fig. 16 Stress-strain curves for ghe impure MRC iron with RRR ~400 at 4.2 K.

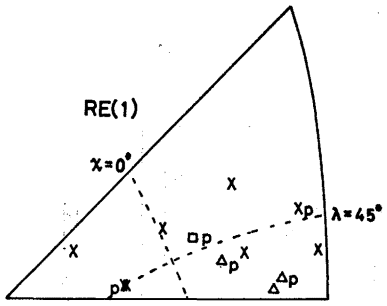

(a) P: 2-3 % at 300 K.

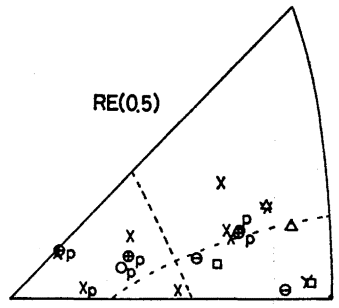

(b) P: 2-3 % at 300 K.

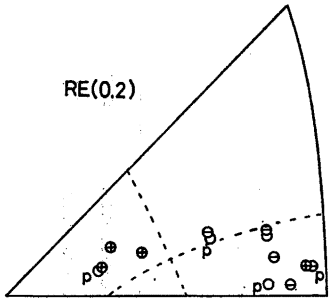

(c) P: less than 1 % at 300 K.

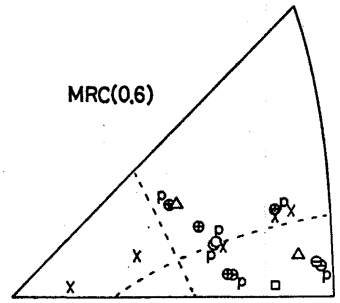

(d) P: 1 % at 300 K.

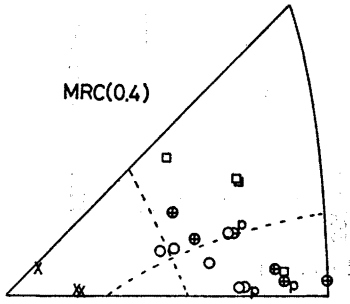

(e) P: 1 % at 300 K.

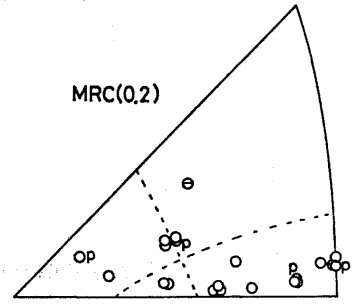

(f) P: 1 % at 300 K.

Fig. 17

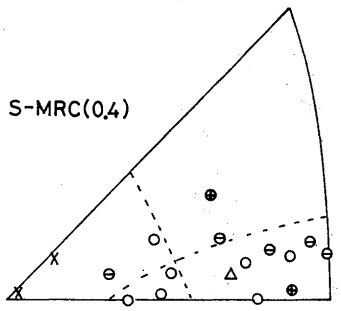

(g) no prestrain

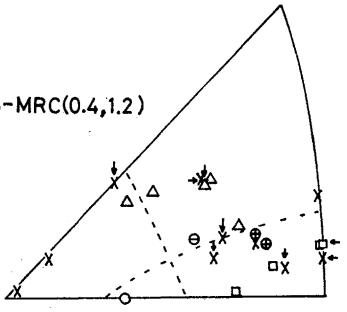

(h) P: 0.5% at 77 K.
arrow: S-MRC(1.2)
no arrow: S-MRC(0.4)

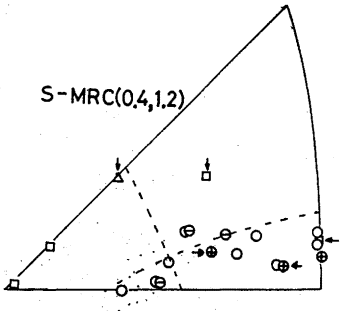

(i) P: 0.5–1% at 300 K.
arrow: S-MRC(1.2)
no arrow: S-MRC(0.4)

Fig. 17 Results in the orientation dependence of the deformation-mode for specimens of various sizes at 4.2 K.

○ slip, ⊖ slip with a few twins, ⊕ slip with many twins, □ twinning, △ twinning and cleavage, × cleavage and P pre-strain

the mode is (1)–(3) for the RE(0.2) specimen and almost (1) for the MRC(0.2) specimen.

From the results mentioned above it is pointed out that slip deformation tends to be easy for the specimen with smaller sizes and orientations near $\chi=0°$.

3.1.3. Observation of surface and inner part of a deformed specimen at 4.2 K

The ability of slip deformation at 4.2 K is closely related with the condition of twin nucleation as mentioned in previous sections. In this section, therefore, the observations of the specimens deformed at 4.2 K

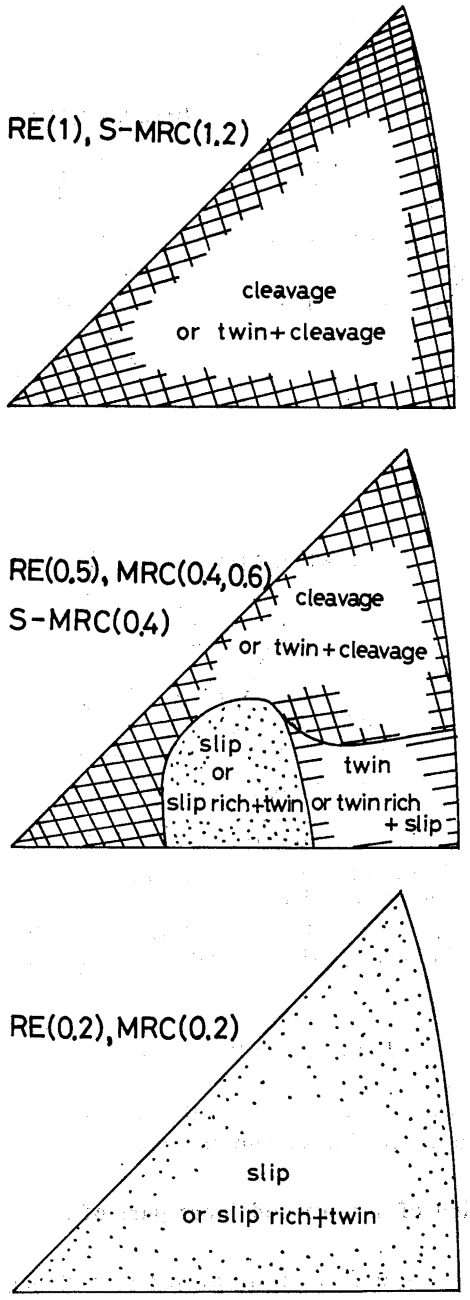

Fig. 18 Deformation-mode maps for specimens of various sizes at 4.2 K.

were made focusing the aspects of twin by means of optical and electron microscopy. Fig. 19 shows the typical aspects of twin trace on the surface of the specimens deformed by twinning or fractured by cleavage. Twins in these specimens had aspects mentiOned below.

i) the width of a twin was more extensively distributed in the specimens of larger sizes and the maximum of the width tended to increase, that is, the width was relatively smaller in those of smaller sizes. The tendency is shown in Fig. 20.

ii) although the specimens of 0.2 mm in diameter were almost deformed by slip, for the RE(0.2) specimen deformed with a few twins the twin trace was too fine to be observed and in fact the traces of micro-twins formed before macro-yielding could not be observed. On the other hand, for impure MRC(0.2) specimen deformed with many twin bursts in the region of flow stress the surface was covered by many fine twin traces (Fig. 19(c)).

iii) in the unstrained specimens many twins and twin intersections were often obseved in comparison with those pre-strained (Figs. 19(a) and (b)). The shape of twin boundary was straight for the unstrained specimens, but was of dentate line for those pre-strained (Fig. (d)).

On the examination of twin structures in the inner part of twinned specimens twin boundaries and stacking faults could not be observed. However, dislocation structures before macro-yielding shown in Fig. 21 could be observed at 4.2 K. This example shows that the dislocations had the component of screw, but some of them were mixed dislocations and the intersections between disloations were observed at many sites. It is pointed out from observation that at a yield point on a stress-strain curve twin dislocations are not generated but slip dislocations are generated being locally concentrated in slip bands.

3.1.4. Orientation dependence of yield stress

The yield stress, τ_y of slip deformation obtaining from the data of the stress-strain curves in RE and MRC irons, is plotted against χ in Fig. 22. The yield criteria were chosen as the flow stress at 0.5% tensile plastic strain for unstrained specimens and the level of plateau stress just after yielding for pre-strained specimens, details of which will be mentioned in a later section. Also, the yield stress denoted in this figure is the shear stress resolved the tensile yield stress on the maximum shear stress plane containing slip direction [111]. Since the yield stress was independent of the specimen size in both RE and MRC irons, the yield stresses of the specimens with different sizes were not specified in the figure. The $\tau_y-\chi$ curve was of asymmetric concave type with minimum at $-10°<\chi\leqq 0°$ and maximum at $\chi=30°$. The ratio of $\tau_y/\tau_{y,\chi=0}$ was constant at temperatures below 90 K and gave the values of 1.12 at $\chi=-30°$ (twinning direction) and 1.22 at $\chi=30°$ (anti-

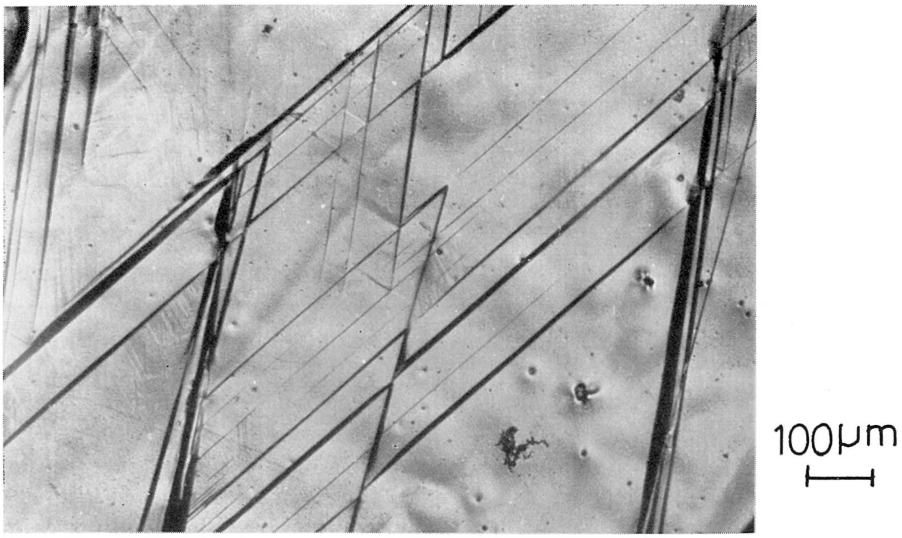

Fig. 19(a) S-MRC(1.2) ($\chi=11°$, $\lambda=37°$) fractured by cleavage.

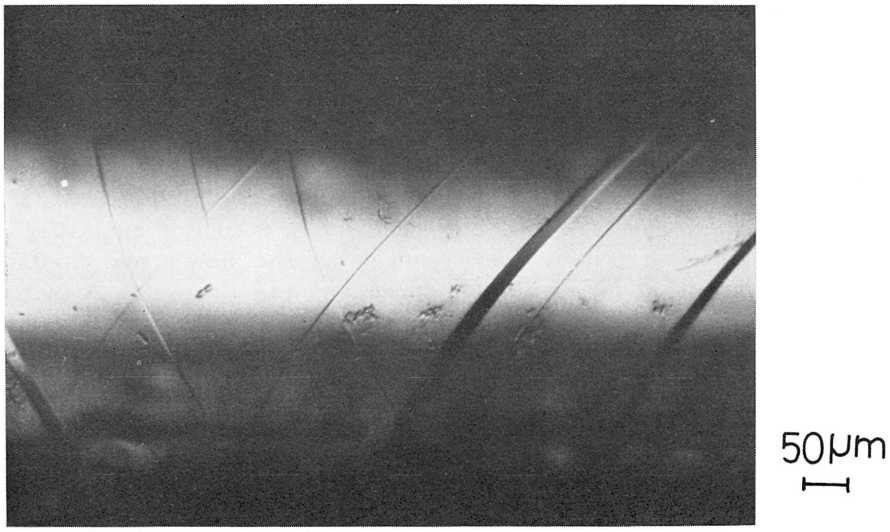

Fig. 19(b) MRC(0.6) ($\chi=21°$, $\lambda=47°$) fractured by cleavage.

Fig. 19(c) Impure MRC(0.2) ($\chi=25°$, $\lambda=37°$) deformed by slip with many twin bursts.

Fig. 19(d) RE(0.5) ($\chi=12°$, $\lambda=45°$) deformed by slip with many twins after pre-straining by 3 % at 300 K.

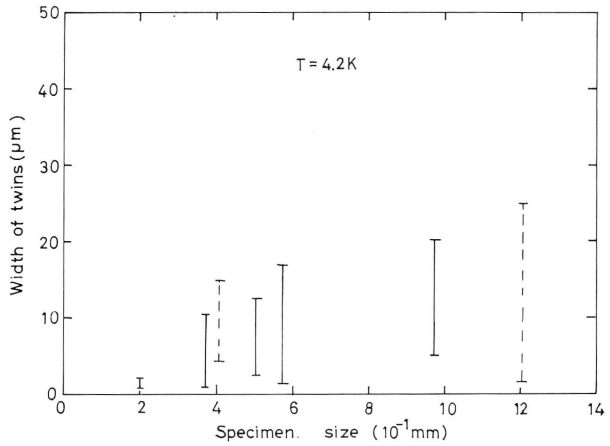

Fig. 20 Relation between the width of twins and the specimen size. The strainght and dash lines indicate wire and sheet specimens, respectively.

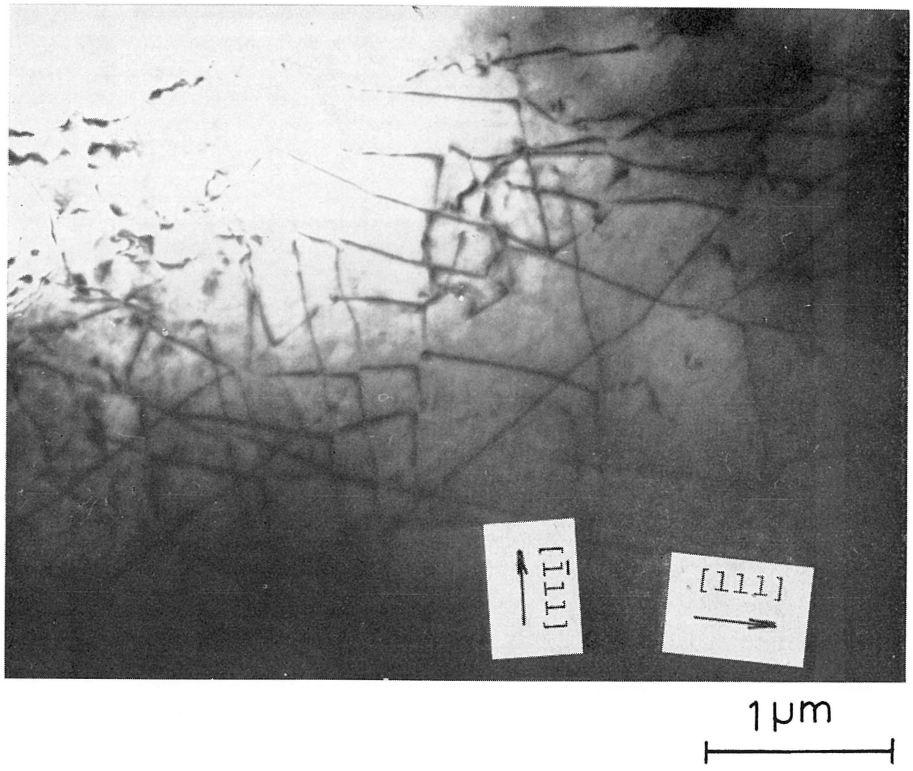

Fig. 21 Dislocation structure in the specimen of S-MRC(1.2) fractured by cleavage before macro-yielding at 4.2K ($\chi=19°$, $\lambda=40°$).

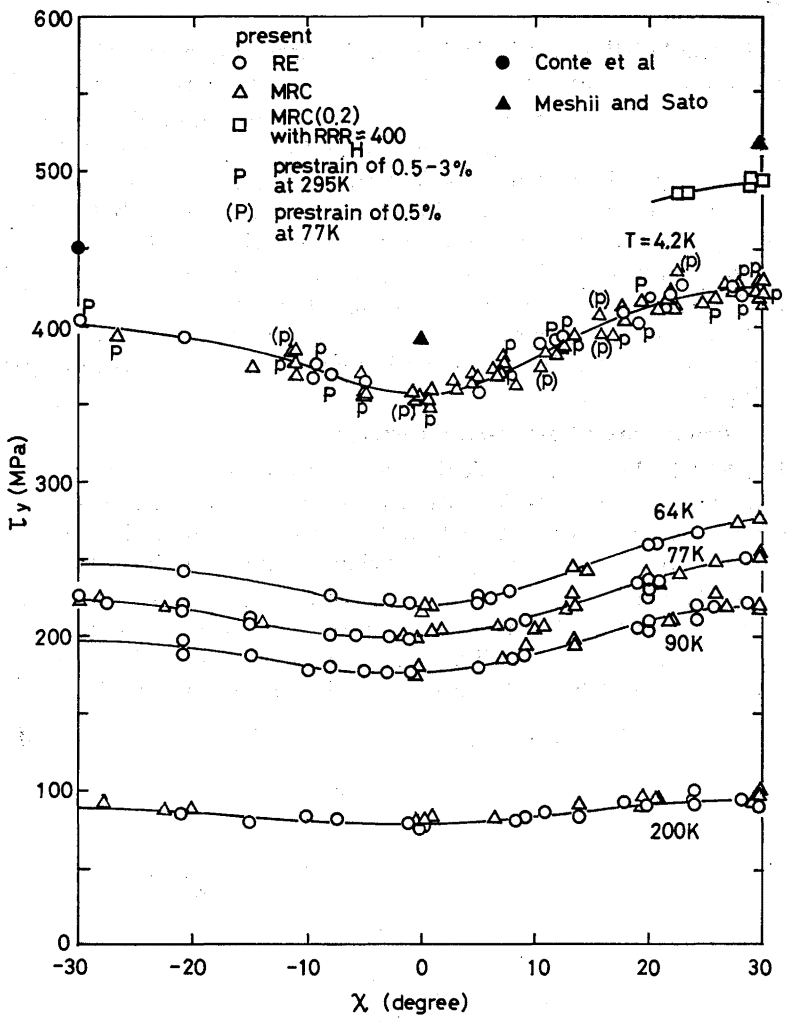

Fig. 22 Relation between the yield stress and χ for various specimens in the temperature range 4.2 to 200 K.

twinning direction). The maximum and minimum of yield stress at 4.2 K were about 425 and 355 MPa, respectively, though the data were scattered. Sato and Meshii[46] have obtained the values of 1.15 and 1.35 at each orientation at 60 K, respectively. Conte et al.[2] ($\chi=-30°$) and Meshii and Sato[3] ($\chi=0°$ and 30°) have obtained the yield stress at 4.2 K as shown in the figure, but their values are higher than those obtained in the present investigation. The yield stress of impure iron with $RRR_H \simeq 400$ was hardened by 65 MPa in comparison with those fully hy-

drogen-treated.

3.2. Characteristics of slip in high-purity iron single crystals

The ability of slip deformation was examined in previous sections from the effect of specimen size and it was experimentally clarified that the specimen of a smaller size could be deformed by slip at 4.2 K. Therefore, it was possible from this fact to investigate various fundamental characteristics of slip deformation in iron down to or below 4.2 K as mentioned below. From a point of view mentioned above, high-purity iron single crystals of MRC of a small size were used in this experiment: MRC(0.2) specimens for obtaining stress-strain curves in a wide temperature range, temperature dependence of yield stress and activation parameters, S-MRC(0.4) for active slip systems and S-MRC(1.2) for dislocation structures.

3.2.1. Behaviours of stress-strain curves

Figs. 23-25 show the typical stress-strain curves for pure iron and Fe-150 appmC. The load-elongation curve was translated into the stress-strain curve on the assumption that the active slip plane is the maximum shear stress plane containing the primary slip direction [111] such as $(\bar{1}01)$ or $(\bar{2}11)$ plane for orientations A or B as shown in Fig. 2, respectively. At 348 and 385 K three-stage hardening occurred for both A and B orientations as shown in Fig. 23, although it is not of large scale as seen in FCC metals[47]. The stress-strain curves in this figure may be

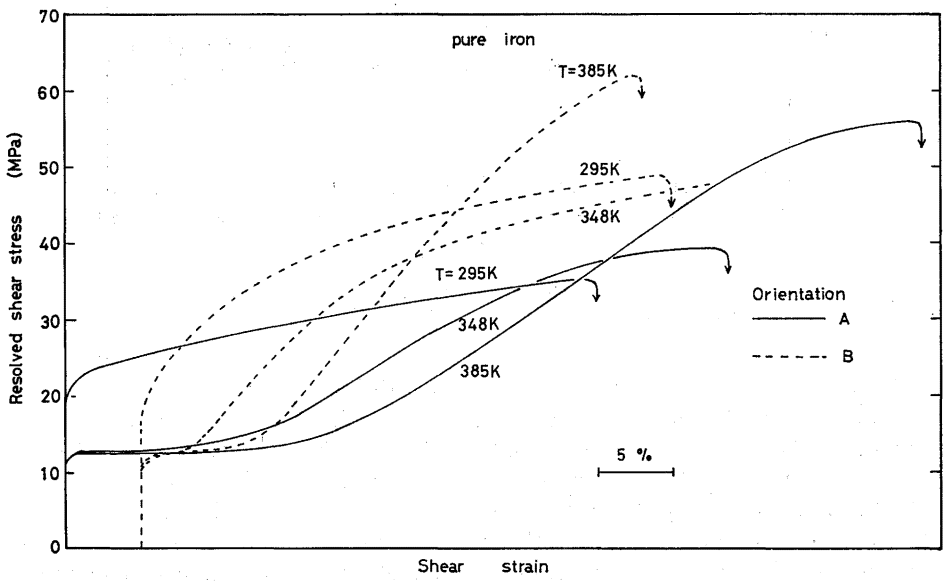

Fig. 23 Stress-strain curves for pure iron at 295, 348 and 285 K.

described as follows: after the initial yielding there is a very short region of high work-hardening rate (Stage 0), then the work-hardening rate decreases to a low constant (Stage I); the work-hardening rate then increases gradually to a region of high constant value (Stage II) followed by a region where the work-hardening rate continuously decreases (Stage III). This three-stage hardening has been reported by Keh and Nakada (at 298 and 327 K)[14] and Spitzig and Keh (at 250 and 298 K)[48] for pure iron single crystals, and Mitchell et al. ($228\,K \leqq T \leqq 373\,K$) for zone-refined niobium single crystals[49].

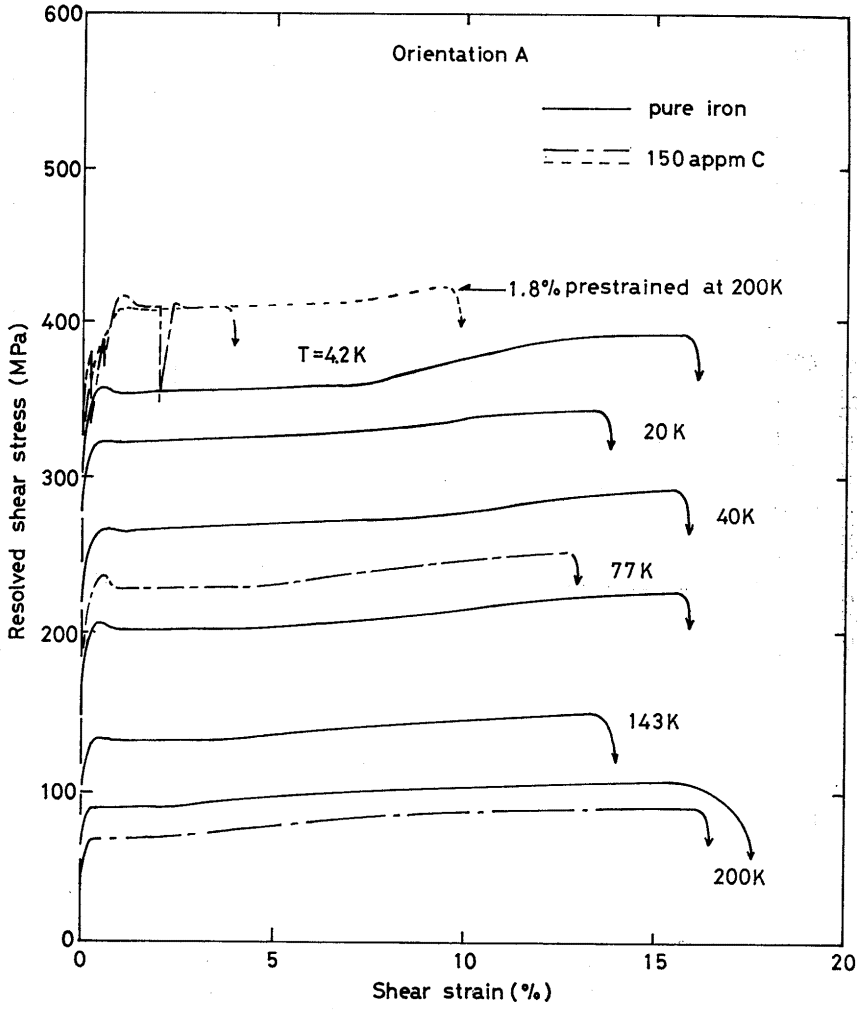

Fig. 24 Stress-strain curves for the pure iron and Fe-150 appmC alloy oriented at (A) below 200 K.

Figs. 24 and 25 show the stress-strain curves in the range 4.2 to 295 K. The three-stage hardening no longer appeared at temperatures below 295 K in the present investigation, although it has appeared in the results by other investigators mentined above. At 295 K the stress-strain curves became parabolic. At intermediate temeratures 143 to 200 K, it exhibited the sharp yield but no yield drop. However, the results by Keh and Nakada and Spitzig and Keh at these temperatures have given the parabolic stress-strain curves and the higher work-hardening rate than those in the present investigation. In the stress-strain curves below 77 K the small yield drop appeared, the yielding was completed

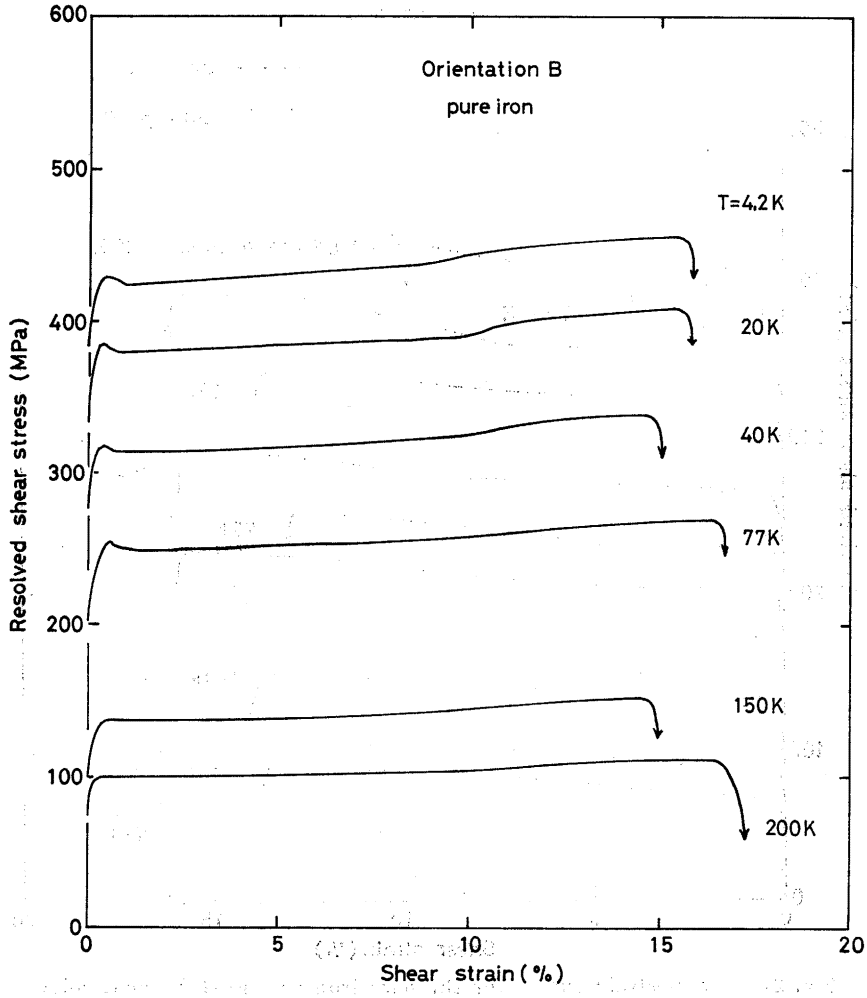

Fig. 25 Stress-strain curves for thepure iron oriented at (B) below 200 K.

within 1 % plastic shear strain (0.5 % tensile plastic strain) and the plateau stress continued up to about 7 % strain. The increase in stress in the range 1 to 7 % strain was below 10 MPa. The elongation was near 15 % strain independently of test temperature and orientation.

There have been a little examples of stress-strain curves in 'pure iron single crgstals' well-annealed so far obtained below 77 K, for example, Tomalin and Stein (20 and 77 K)[50], Keh and Nakada (77 K)[14], Spitzig and Keh (77 K)[48], Sato and Meshii (60 K)[46] and Quesnel et al. (77 K)[51]. However, there have not yet been any examples at 4.2 K besides this investigation. The specimens used by above investigators were all of plates and were purified in a ZrH_2 system.

In the stress-strain curve for Fe-150 appmC in Fig. 24 the stress level is higher at 4.2 and 77 K and lower at 200 K in comparison with pure iron of the same orientation, which exhibiting the phenomena of solution hardening and softening due to carbon atoms. The feature of the stress-strain curves for Fe-150 appmC, however, was almost similar to that for pure iron except the characteristics such as the slightly large yield drop, the appearance of twinning and the small elongation at 4.2 K. Moreover, the pre-straining at 200 K enhanced the elongation at 4.2 K and there was no change in the yield stress due to pre-straining.

3.2.2. Temperature dependence of yield stress

The choice of yield criteria is a matter of importance upon the investigation of the mechanical properties in materials. For example, in case of the parabolic stress-strain curve without clear yield drop the choice of yield criteria exerts great influence upon the value of yield stress and moreover the feature of the temperature dependence of yield stress.

Quesnel et al.[51] examined various yield criteria such as (1) proportional limit, (2) extrapolation of linear work-hardening to the elastic line, (3) lower yield stress, (4) constant plastic strain offset, (5) constant plastic strain-rate and (6) constant activation volume. It was found from their investigation that the strain which the plastic strain-rate was constant at the first time, was 0.5 % tenslie plastic strain for the parabolic stress-strain curve, which satisfying two criteria (4) and (5). Criterion (5) means the beginning of the steady state flow on plastic deformation. In case of the appearance of yield drop the criterion (3) is used. Also, in the present investigation the plastic flow in steady state seems to begin near 0.5 % plastic strain (1 % shear strain) at all temperatures as seen from the stress-strain curves in Figs. 23-25. Accordingly the stress at 0.5 % tensile plastic strain was chosen as the yield criterion. As regards the choice of yield criteria for the specimens deformed at lower temperatures after pre-straining at a higher temperature, the plateau stress just after roundly yielding was chosen as the yield stress because this stress level was equal to that at 0.5 % tensile

plastic strain for the specimen with no pre-strain as shown in previous sections and in Fig. 24 for Fe-150 apmmC. Therefore, the yield stress of Fe-150 appmC below 77 K were obtained from the flow stress at 0.5 % tensile plastic strain for the specimens pre-strianed by about 0.5 % tensile plastic strain at 200 K. The reason for pre-straining is to observe the deformation due to the motion of free dislocation and the homogeneous deformation at lower temperatures. The yield stress referred in Figs. 27-29 were also determined from the yield criterion mentioned above. The tensile yield stress, furthermore, was resolved on the maximum shear stress plane. The experimental results with regard to real slip plane will be mentioned in a later section.

The variation in the yield stress as a function of temperature and orientation is shown for pure iron and Fe-150 appmC in Fig. 26. The feature of the temperature dependence of yield stress for pure iron was

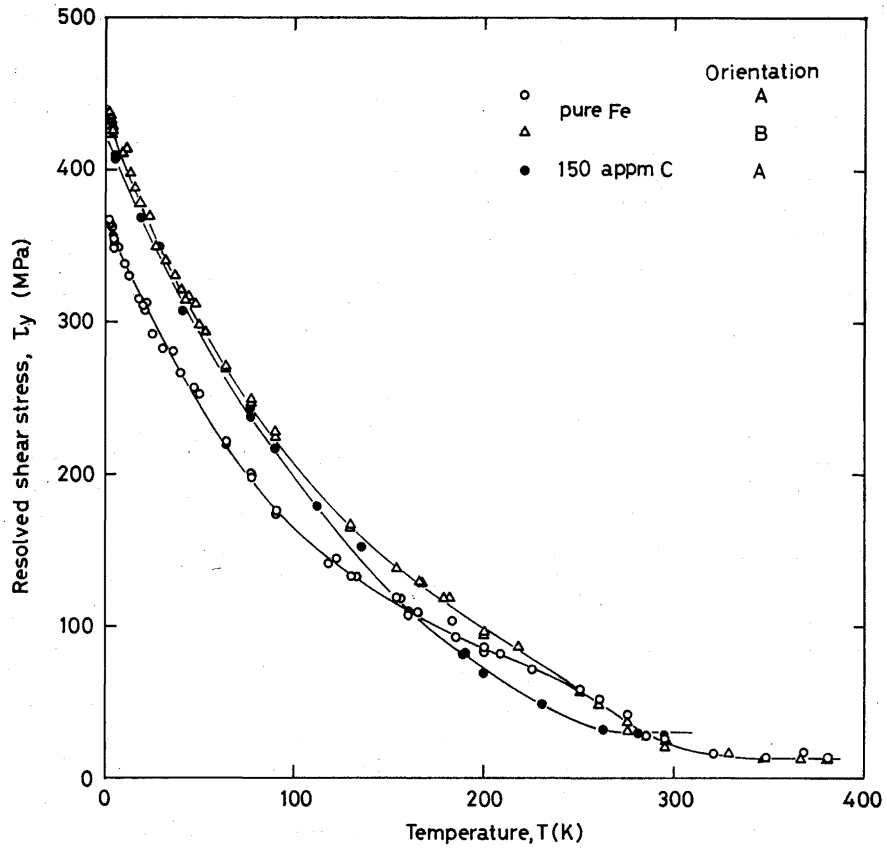

Fig. 26 Temperature dependence of the yield stress for pure iron and Fe-150 appmC alloy.

a weak S character, being especially remarkable in orientation A. Above 340 K there was a plateau stress, i.e. the athermal region of yield stress, in which the value of yield stress was 15 MPa independently to orientation. When temperature decreased down to 200 K, the rapid increase in the yield stress occured in the range 200 to 300 K in orientations of both A and B. Namely, there appeared a hump (concave down region) on the yield stress-temperature curve ($\tau_y - T$ curve) in this range. When temperature, moreover, decreased down to 0.7 K, the yield stress of pure iron monotonously increased after the increasing rate of yield stress reversed around 200 K (an inflection point on $\tau_y - T$ curve), in orientations of both A and B.

As regarding the orientation dependence of yield stress, the difference between orientations A and B became gradually large with decreasing temperature below 250 K and the ratio of yield stress, $\tau_{y,A}/\tau_{y,B}$ calculated from Fig. 26 was almost constant 1.22 at temperatures below 90 K.

The addition of the small amount of carbon atoms to high-purity iron remarkablly changed the feature of the temperature dependence of yield stress in pure iron: the temperature dependence of a weak S character which appeared in pure iron, disappeared and the yield stress resulted in the monotonously decreasing function of temperature. In comparison with pure iron in the same orientation A, the yield stress of Fe-150 appmC was lower in the intermediate temperature region (softening) and higher at temperatures below 160 K (hardening). This nature of Fe-150 appmC alloy is similar to that of pure iron used by Stein and Low[10)11)] and Spitzig and Keh[48)] as refered in Fig. 27. Their iron single crystals were purified in a ZrH_2 system and especially the specimens used by Stein and Low were reported to contain only less than 5×10^{-3} wppm carbon. However, the stress-strain curve at 77 K obtained by them exhibited twinning in the early stage of deformation and then parabolic curve by slip. The stress-strain curve at 77 K in the present investigation was not parabolic and exhibited the plateau stress region following a small yield drop. Moreover, the data by Meshii and Sato[3)] and Quesnel et al.[51)] using the single crystals of thin plate were in good accord with the present ones at intermediate temperatures but were different below 130 K. Quesnel et al. have explained that the hump appearing in the intermediate temperature range resulted from the extrinsic hardening due to hydrogen remaining in their specimens after ZrH_2-treatment. For examining the effect of hydrogen, H_2-purified specimens in the present investigation were annealed in vacuum of 1.3×10^{-4} Pa at 300℃ for 30 min to remove hydrogen which may remain in the specimens. The result is shown in Fig. 28, which shows the enlargement of $\tau_y - T$ curve in the intermediate temperature range in Fig. 27. The result accorded with that for as H_2-purified specimens. This means that the

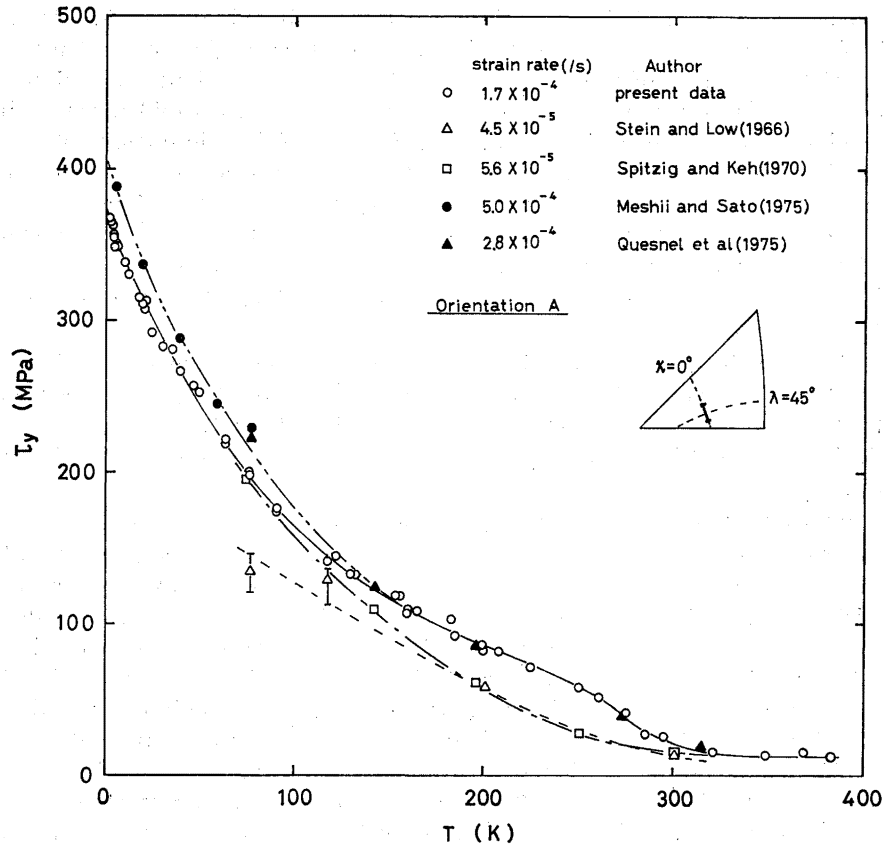

Fig. 27 Temperature dependence of the yield stress for the pure irons in the present result and reported by other investigators.

hump does not result from the effect of hydrogen atoms, but is intrinsic nature of iron. In the same figure is shown the results reported by Matsui et al. using the coarse-grained iron of the bamboo type with $RRR_H \simeq 3600$ and more than 5000. In their data the hump appeared in the same temperature as the present data and the scale of the hump depended on purity. It is not clear from their experimental results that the purity dependence of the hump occurs or not in iron single crystals of higher purity than $RRR_H=4000$ in the present investigation because their result is due to polycrystals. The appearance of this hump has been also reported by Diehl et al. (single crystals)[52] and Tseng and Tangri (polycrystals)[53]. In general it could be concluded that the hump has been observed only for high-purity iron reducing sufficiently both gas and metallic impurities.

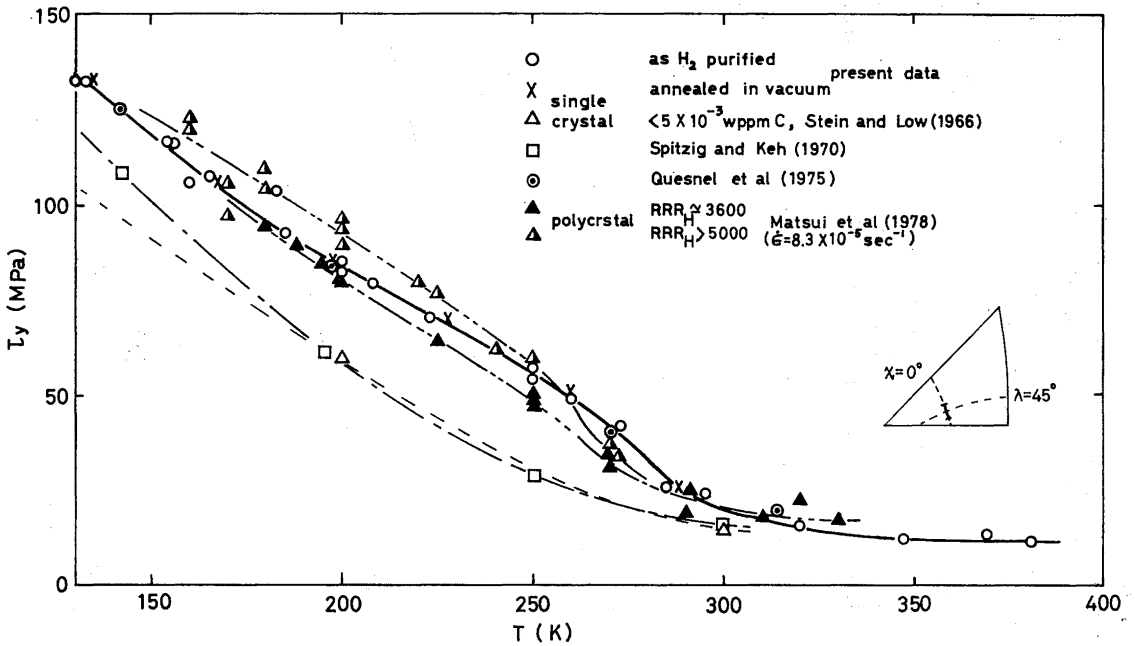

Fig. 28 Temperature dependence of the yield stress for the pure irons in the present result and reported by other investigators in the intermediate temperature range.

The enlargement of $\tau_y - T$ curve at very low temperatures below 30 K in Fig. 26 is shown in Fig. 29. In the present investigation the yield stress is evaluated down to 0.7 K and monotonously increased with decreasing temperature. There are very examples of success of slip deformation at very low temperatures as mentioned in section 3.1. Moreover, it is only results by Meshii and Sato and Matsui et al. except the present data that the $\tau_y - T$ curve was obtained down to helium temperature. Altshuler and Christion (polycrystals)[13] and Tangri and Lloyd (polycrystals)[54] recorded the twinning stress below 10 and 20 K, instead of the yield stress for slip, respectively. The yield stress by Meshii and Sato in the figure is larger than the present result in any orientation. That by Matsui et al. is in good accord with the present ones though the values of yield stress are scattering around helium temperature.

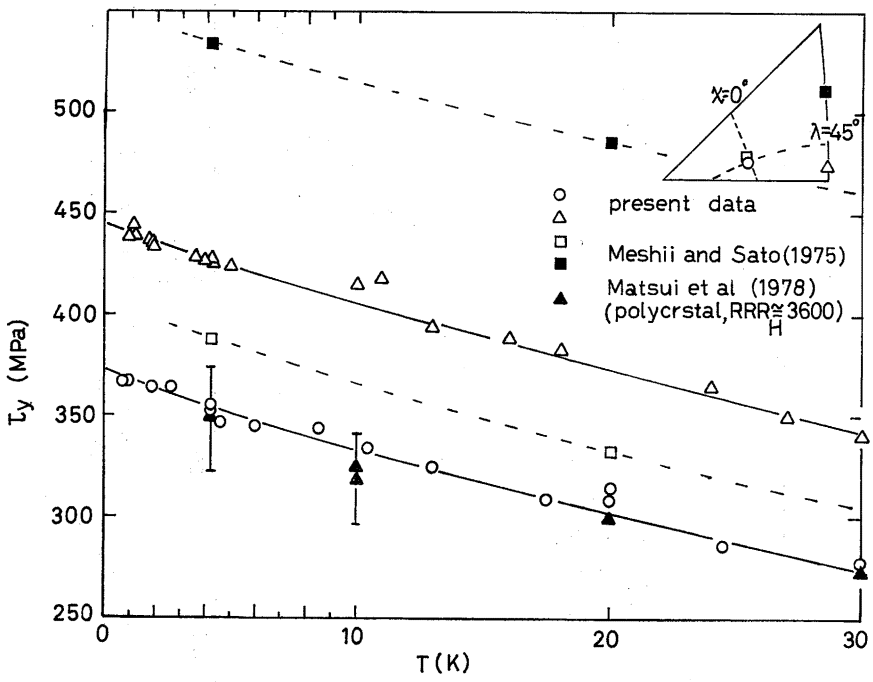

Fig. 29 Temperautre dependence of the yield stress for the pure irons in the present result and reported by other investigators in the very low temperature range.

3.2.3. Activation parameters

The strain-rate sensitivity, β obtained from stress relaxation technique (above 4.2 K) and strain-rate change test (below 4.2 and partly up to 77 K) is plotted against temperature in Fig. 30. The definition of β

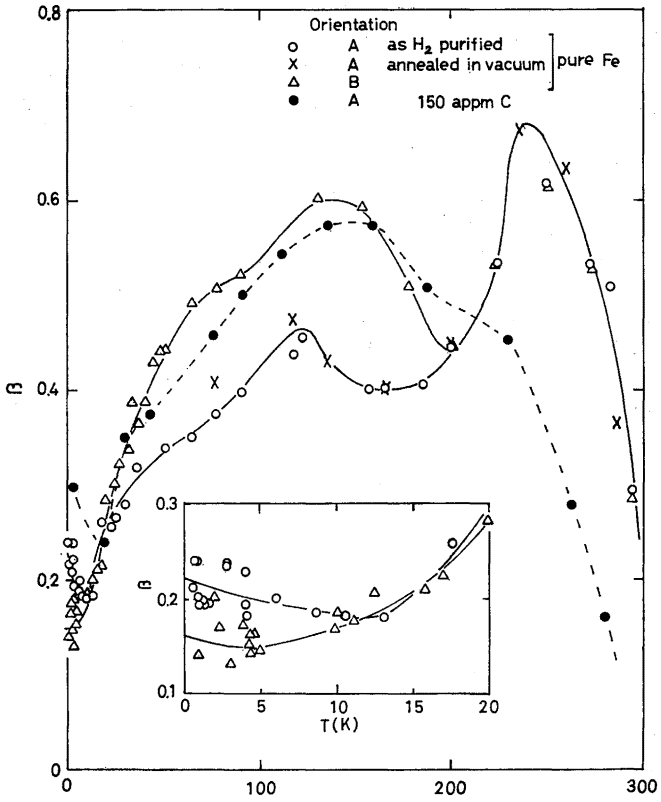

Fig. 30 Temperature dependence of the strain-rate sensitivity for pure iron and Fe–150 appmC alloy.

is given in Appendix. The feature of $\beta-T$ curves for pure iron is of asymmetric camel-hump type with a minimum at 180 and 200 K in orientations A and B, respectively. These minima and a maximum around 250 K roughly correspond to the inflection points and a maximum slope on τ_y-T curves in Figs. 26 and 28, respectively. The orientation dependence of β appeared only in the range below 200 K in orientations of both A and B. The results for high-purity iron in the present investigation is very different from those obtained before the year 1970 by investigators such as Basinski and Christian[5], Conrad and Frederik[6], Nakada and Keh[55] and Spitzig and Keh[15]. Their $\beta-T$ curves have shown the feature of convex type with a maximum around 150 K, which is very similar to that for Fe–150 appmC alloy in this figure. The values of β in specimens annealed in vacuum after H_2-purification sufficiently fitted with that in specimens as H_2-purified. The characteristics of β for pure iron mentioned above, therefore, are not due to hydrogen atoms but are the

intrinsic nature of iron. It should be, moreover, noted that the strain-rate sensitivity does not tend to zero but seems to have a non-vanishing value at absolute zero temperature for both pure iron and Fe–150 appmC alloy. The values of β obtained from the stress relaxation test and strain-rate change test were equal each other in the low temperature range below 77 K.

The activation area, A^* calculated from the strain-rate sensitivity and eq.(A 13) in Appendix is plotted against the yield stress in Fig. 31. The $A^*-\tau_y$ curve in pure iron had a peak at the stress level about 100 MPa independently of orientation. This peak corresponds to the inflection point on τ_y-T curves in Figs. 26 and 28 and the minima on the $\beta-T$ curve in Fig. 30. The orientation dependence of $A^*-\tau_y$ relationship appeared above the stress level of 130 MPa. The value of A^* did not change by annealing in vacuum after H_2-purification. The $A^*-\tau_y$ curve for Fe-

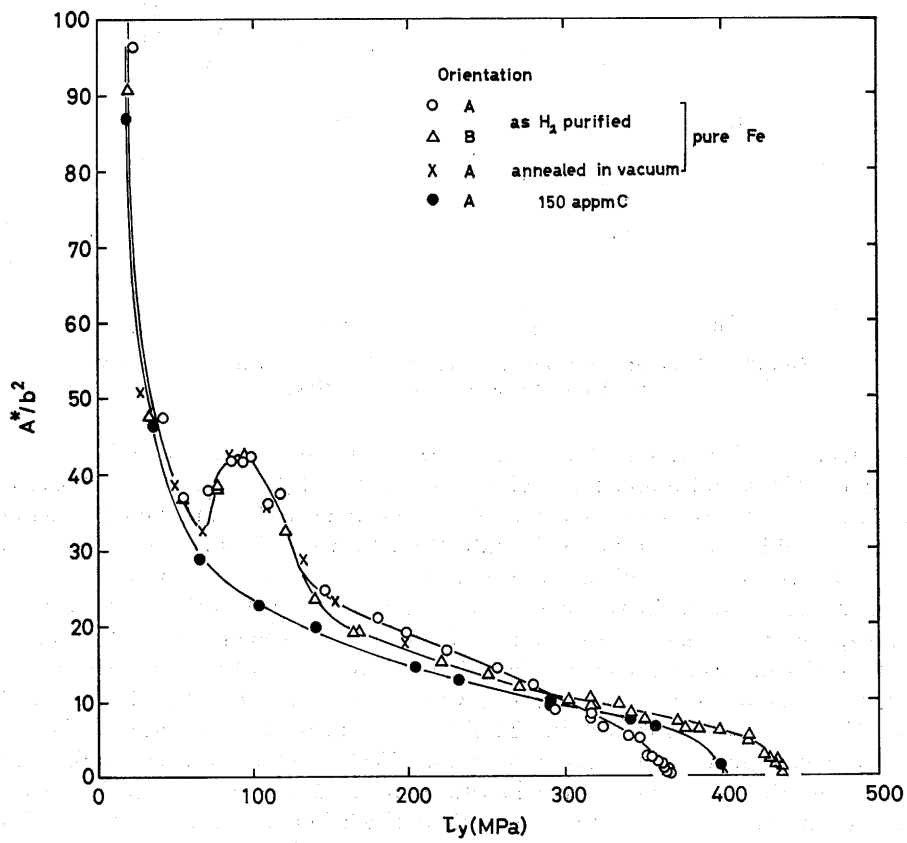

Fig. 31 Stress dependence of the activation area for pure iron and Fe–150 appmC alloy.

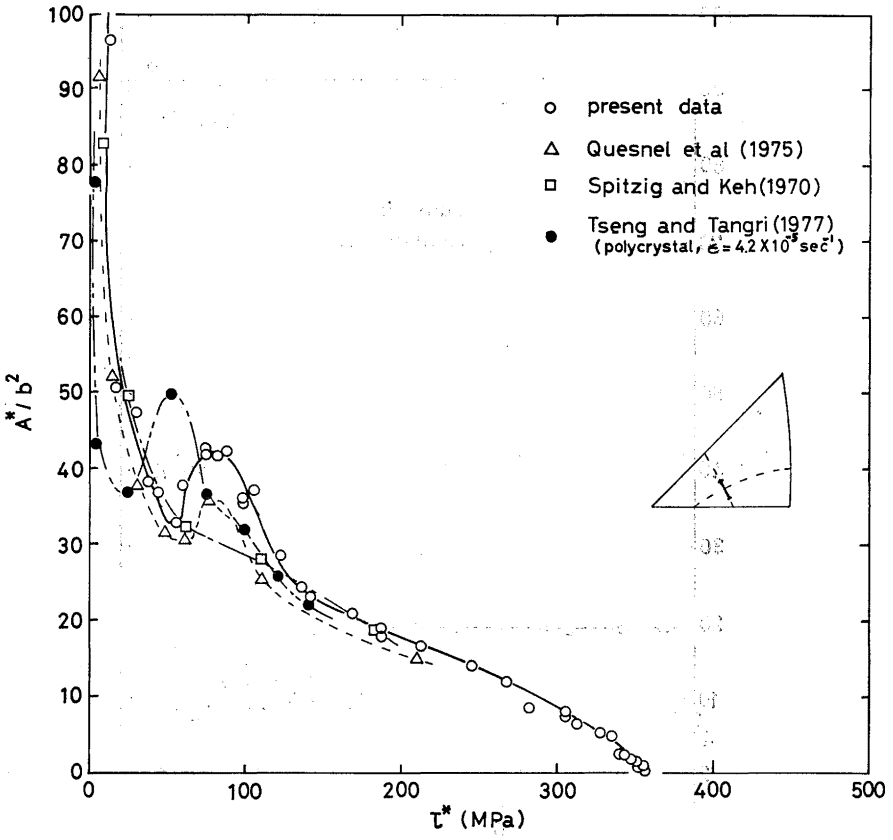

Fig. 32 Stress (effective stress) dependence of the activation area for the pure irons in the present result and reported by other investigators.

150 appmC alloy was the monotonously decreasing function of stress and did not exhibit any peak of A^*. In high stress region (very low temperature range) the activation area rapidly decreased with increasing the yield stress and approached zero value at the stress near absolute temperature in both pure iron and Fe-150 appmC alloy.

Fig. 32 shows the $A^*-\tau^*$ relation obtained by other investigators. The effective stress, τ^* was obtained by subtracting the athermal stress from the yield stress. It is found from this figure that for the data which have a hump on τ_y-T curve, the peak of activation area necessarily appears, which means the correspondence between the hump and the peak.

The strain dependence of activation area is shown in Fig. 33 for pure iron in orientation A as an example. The activation area seems to be independent of strain or dislocation structure all over the tempera-

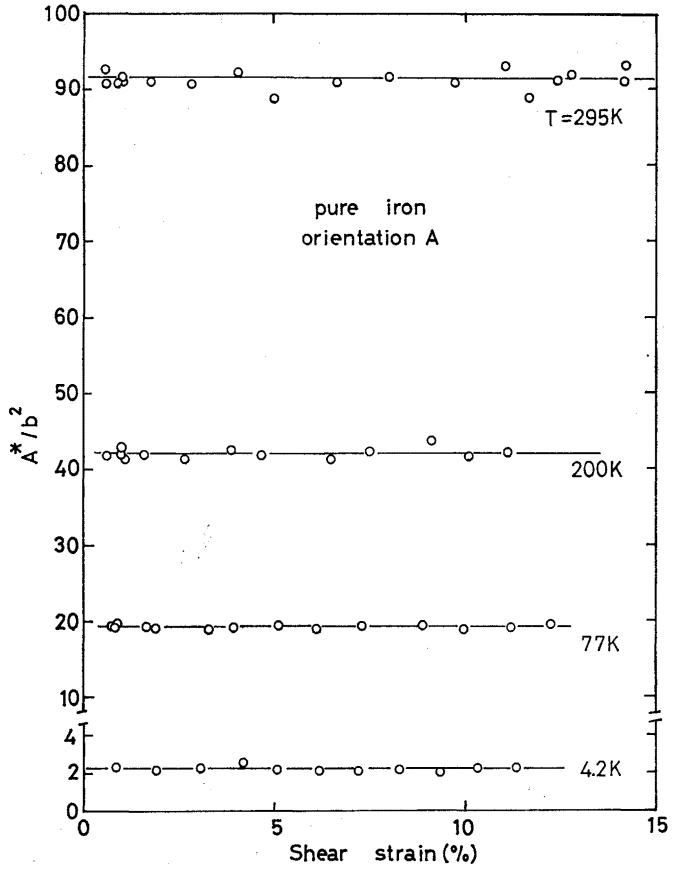

Fig. 33 Strain dependence of the activation area for pure iron at various temperatures.

tures below 300 K. These values were obtained from stress relaxation, but those from strain-rate change test generally depend on strain above 200 K (for example, the result by Spitzig and Keh[15]), which probably results from the change in dislocation structure at a high strain during strain-rate change.

The activation enthalpy calculated by use of eq.(A 4) in Appendix is plotted against temperature in Fig. 34. The scattering of data at higher temperature results from the difficulty in precise measurement of the slope of $\tau_y - T$ curve in the range so that the hump appears. Although one considering the experimental errors mentioned above, the linearity through the origin established in the $\Delta H - T$ relation in the temperature range above~30 K with the slope of about 26 for pure iron, independent of orientation and ~90 K with that of about 30 for Fe-150 appmC alloy.

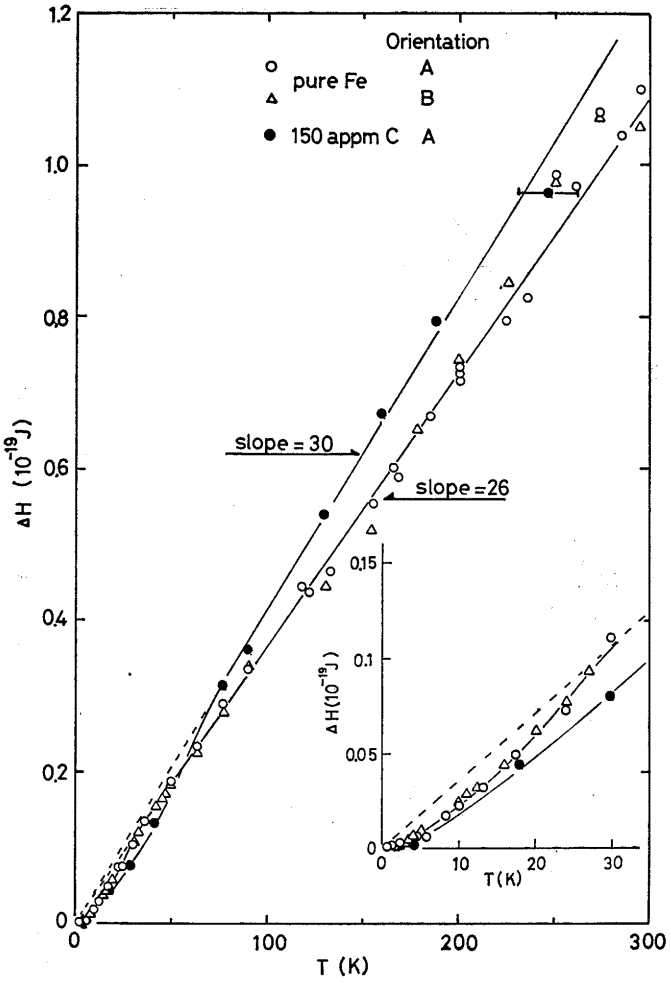

Fig. 34 Temperature dependence of the activation enthalpy for pure iron and Fe-150 appmC alloy.

The constancy of the slope has been so far reported by Basinski and Christian[5], Nakada and Keh[55], Alshuler and Christian[13], Okazaki et al.[56] and Cuttu et al.[57] with the constant value of 26±1, respectively. The values of activation enthalpy, however, deviated downward from the linear line below 30 K. This anomaly in $\Delta H-T$ relation is made clear by plotting the slope in $\Delta H-T$ relation, i.e. the exponential factor, $\Delta H/kT$ in Arrhenius rate equation neglecting the change in entropy term against temperature as shown in Fig. 35. The values of $\Delta H/kT$ rapidly decreased below 30 and 90 Kfor pure iron and Fe-150 appmC alloy, respe-

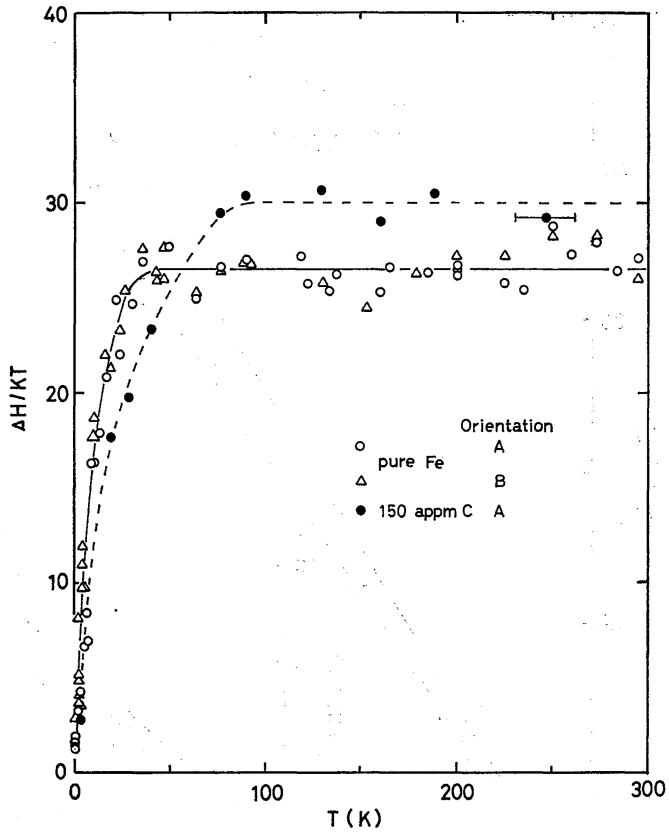

Fig. 35 Relation between $\Delta H/kT$ and temperature for pure iron and Fe-150 appmC alloy.

ctively. Fig. 36 shows the stress dependence of activation enthalpy. The feature of $\Delta H-\tau_y$ curves are very similar to that of τ_y-T curves except the results at very low temperatures. This can be considered from the interrelation between ΔH and T mentioned above.

3.2.4. Active slip systems

The sheet specimens with various orientations were deformed at 4.2, 77 and 200 K and slip lines were observed. At 200 K slip lines could not be observed though specimens were heavily deformed until fracture. At 77 K slip lines were observed for the first time at more than 10 % shear strain as seen in Fig. 37. Slip lines were generally parallel each other all over the surface of specimens, sometimes stopped on the way and were slightly wavy. Slip planes at an orientation of $\chi=30°$ were determined from the observation of slip lines as $(\bar{1}01)$ and $(\bar{1}\bar{1}0)$ planes containing primary slip direction [111] and non-crystalographic plane near

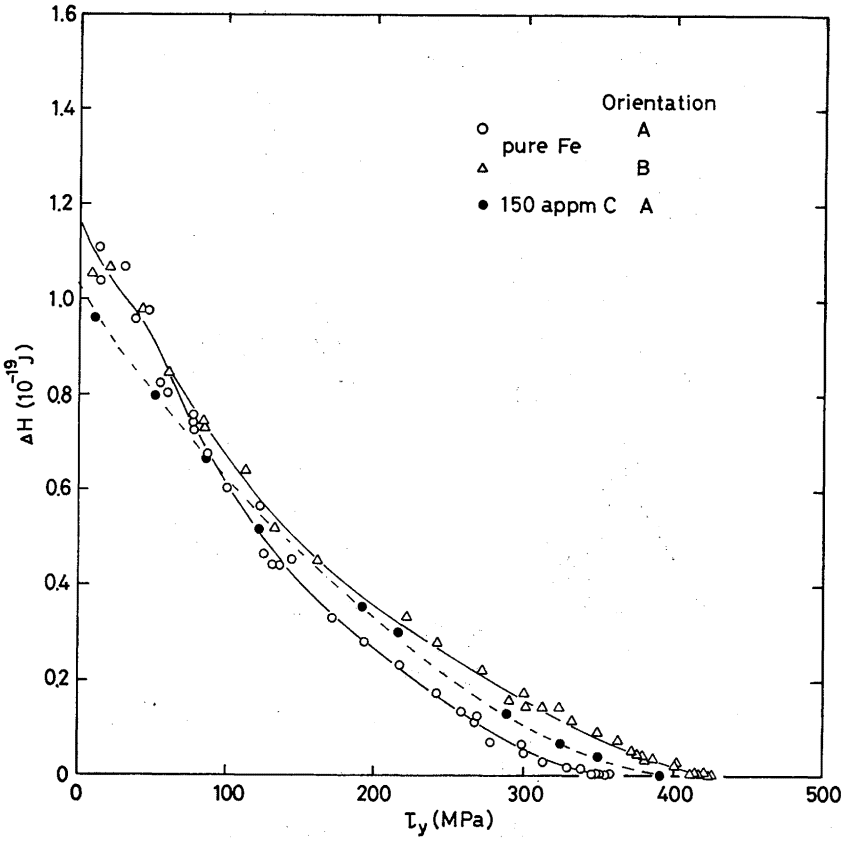

Fig. 36 Stress dependence of the activation enthalpy for pure iron and Fe-150 appmC alloy.

(101) plane containing secondary slip direction [$\bar{1}11$] on the average, at 77 K. At orientations near $\chi=0°$ slip lines were straight and slip plane was ($\bar{1}01$) plane. At an intermediate orientation and $\chi=-30°$, ($\bar{1}01$) plane was determined as a slip plane.

Since most of sheet specimens were not deformed by slip because of twinning and cleavage fracture at 4.2 K mentioned in section 3.1, some of specimens were strained by more than 4 % after pre-straining of 1 % at 77 K. The observation at 4.2 K is shown in Fig. 38. In the specimens pre-strained at room temperature, however, slip lines were not observed although specimens were strained by more than 14 %. The distribution of slip bands for both specimens unstrained and pre-strained were not uniform and it was not also recognized that slip bands were concentrated near the chucked part. Slip lines at 4.2 K were straight and parallel

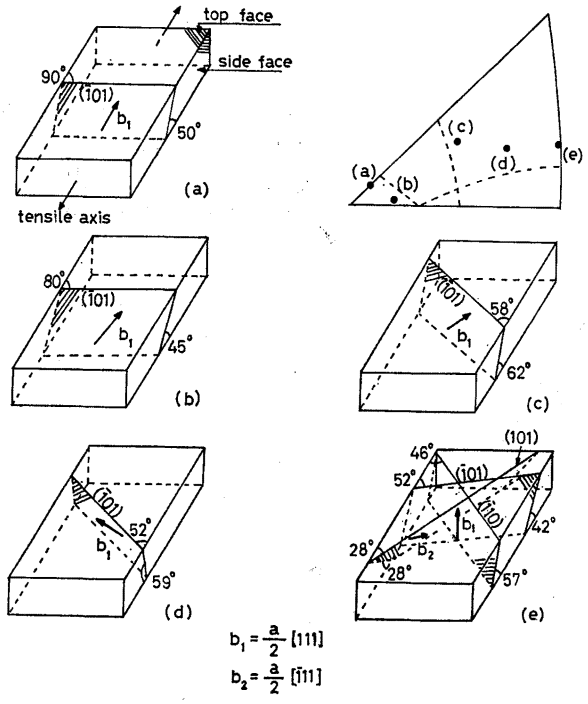

Fig. 37(i) Orientations of the sheet specimens used in the tensile test at 77 K and the geometry of slip plane and Burgers vector.

each other. Although slip plane was not determined at $\chi<-12°$ because of twinning and cleavage fracture, it was $(\bar{1}01)$ plane. Especially, slip planes at $\chi=30°$ were determined to be $(\bar{1}01)$ and $(\bar{1}\bar{1}0)$ planes of primary slip system and (101) plane of secondary slip system. At orientations near the [001]-[011] line $(\bar{1}01)$ and (101) planes were observed together.

The $\phi-\chi$ relation at 77 and 4.2 K is shown with the $\tau_y-\chi$ relation in Figs. 39 and 40. The relation was $\phi=0°$ at both tempratures. The relation at 200 K, which were not obtained in this investigation, have been reported to be $\phi\sim\chi$ by Spitzig and Keh[26] and Matsui et al.[58]. In consideration of this fact, it is thought that the slip plane in iron tends to approach $(\bar{1}01)$ plane as temperature is lowered and becomes $(\bar{1}01)$ plane at 4.2 K. Therefore, it is seen from the results mentioned above that fundamental slip plane is $(\bar{1}01)$ plane.

3.2.5. Observation of dislocation structures

The sheet specimens with width of 1.2 mm were strained by 2% at 30 and 200 K for observing dislocation structures. The photographs are

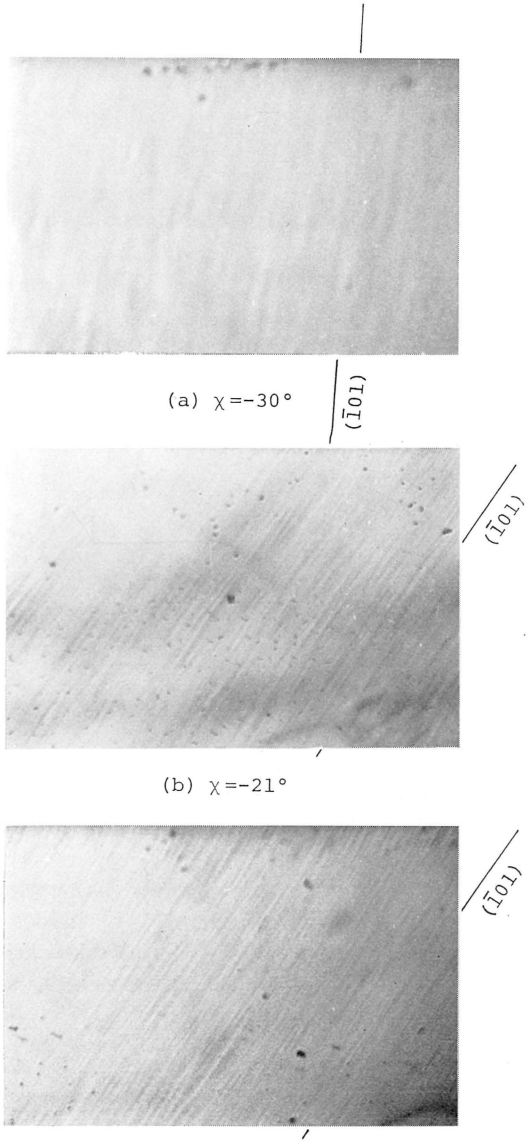

Fig. 38(ii)

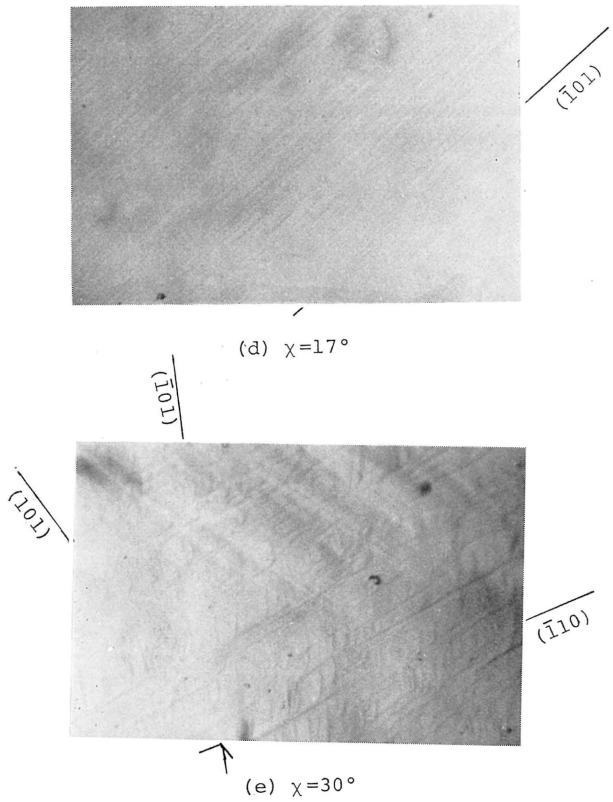

Fig. 37(ii) Slip patterns on the top faces of the specimens of pure iron at 77 K (more than 10 % shear srain, × 400).

shown in Fig. 41. At both temperatures screw dislocations were dominent and two slip systems were active. The [111] dislocations in primary slip system were more dominent at 30 K. Total dislocation density was 3.0×10^8 and $5.2\times10^8/cm^2$ at 30 and 200 K, respectively, and was, therefore, almost independent of temperature. Dislocation loops and debris were more observed at 30 K than at 200 K. These results are in good accord with those down to 77 K reported by other investigators[59)60)].

4. Discussion and conclusion

4.1. Effect of specimen size on deformation-mode at very low temperatures

It is clear from the experiment results that the different in the spe-

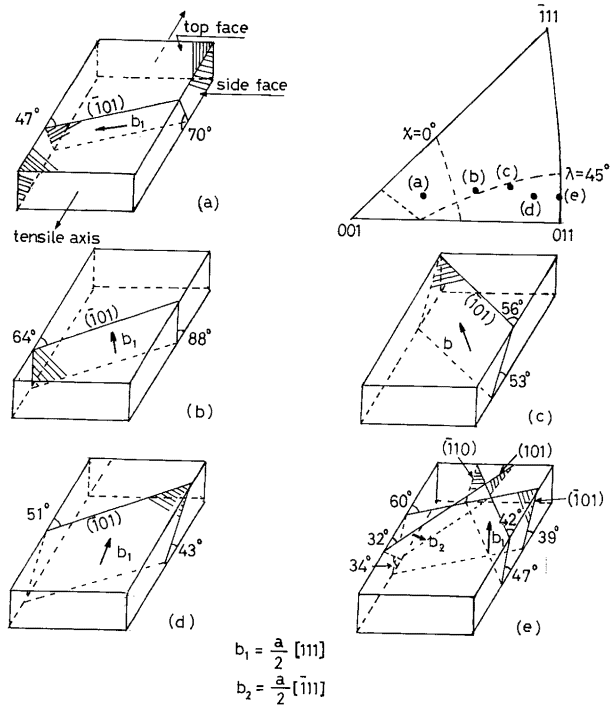

Fig. 38(i) Orientations of the sheet specimens used in the tensile test at 4.2 K and geometry of slip plane and Burgers vectors.

cimen size gives much influence on deformation-mode. This can be explained as a effect of suppression of twinning due to the reduction of specimen size, which is important effect besides well-known purification and pre-straining. This effect is contradictory to the traditional assertion that a definite twin stress essentially exists in twin formation. Actually, the stress at which a twin nucleates is higher than that of slip because the experiment gives the stress-strain curves only by slip down to 0.7 K. The tiwn nucleation at a low stress level in the past may be due to the local structure in the inner of a specimen which depend on the foreign condition. If cleavage fracture is considered to be led by twinning, the ductile-brittle transition temprature will not also have any essential meaning in high-purity iron single crystals.

The formation of a deformation twin can be envisaged as occuring in two stage: (i) nucleation of an embryo, and (ii) its subsequent growth into a macroscopically observable twin. Basically, two different approaches have been adopted to rationalize the nucleation of twins: heterogeneous[61)~65)] and homogeneous nucleation[66)]. At present, the former

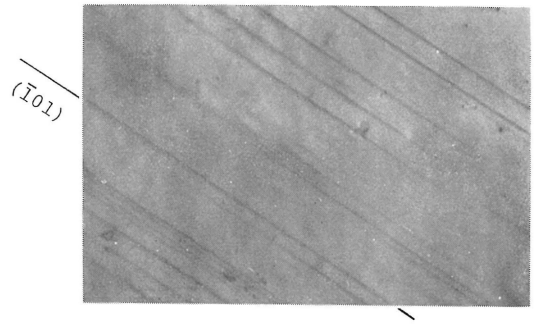

(a) $\chi = -12°$

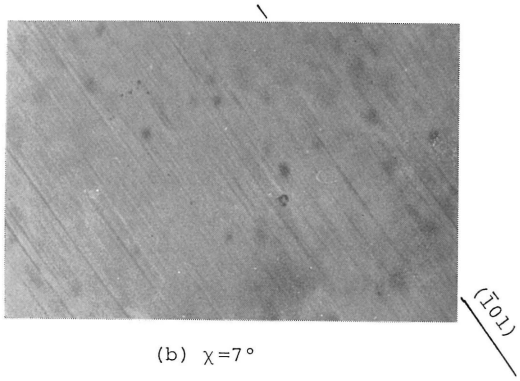

(b) $\chi = 7°$

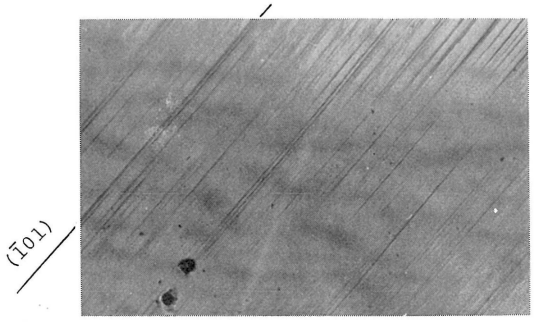

(c) $\chi = 15°$

Fig. 38(ii)

(d) χ=19°

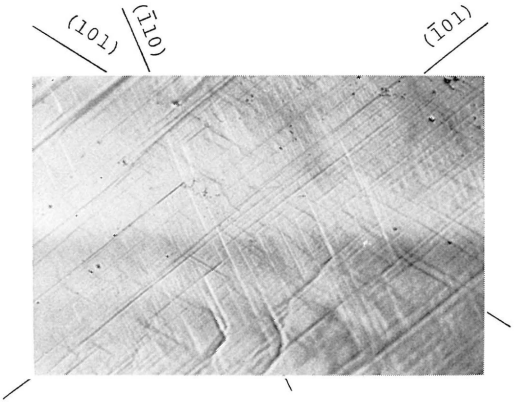

(e) χ=30°

Fig. 38(ii) Slip patterns on the top faces of specimens of pure iron at 4.2 K (about 4 % shear strain, × 400). The specimens oriented at (b) and (c) are not pre-strained at 77 K, while the others are done by 1 %.

have been rather supported in BCC metals from many observations by electron microscope[65)67)~73)]. It is this standpoint that a twin can nuleate from a heterogeneity such as a particular dislocation arrangement. As a source dislocation for twin formation, which is resolved into three partial dislocations (twin dislocations) at a higher stress level as a twin embryo, Sleeswyk[63)], Ogawa[64)] and Levonmaa and Lindroos[72)] have supported a screw, edge and mixed dislocation, respectively. Twin dislocations have been actually observed by electron microscope (for example, a reference[73)] for iron). Vitek[74)] have reported from computer simulation that the stacking faults of three layers was stable in BCC metals and the stress for nucleation of twin dislocations from a screw dislocation

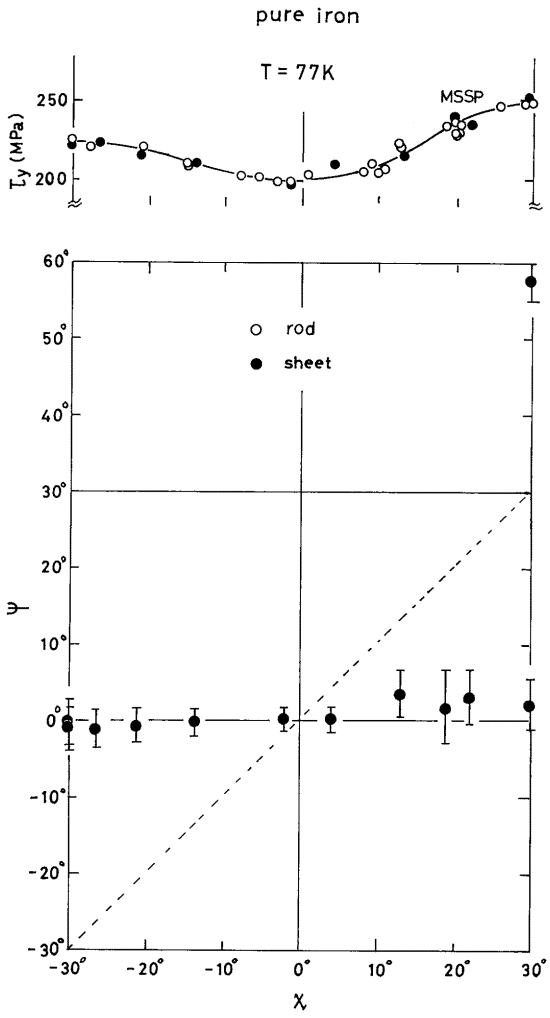

Fig. 39 τ_y—χ and ϕ—χ relations for pure iron at 77 K.

was about 0.03 μ, where μ is shear modulus[75]. This stress is very high and must be realized by high internal stress at local sources of stress concentration, which for example is thought such as small inclusions, sub-boundaries and insular grains, etc. However, these inhomogeneities in a specimen may not exist in our high-purity single crystals. Therefore, the plie-up effect of the group of dislocations is suggested. If the the motion of non-screw dislocations is dominent before macro-yielding and therefore the pile-up of edge dislocations occurs in the inner of local slip bands, the state of very high stress will be formed at a head of

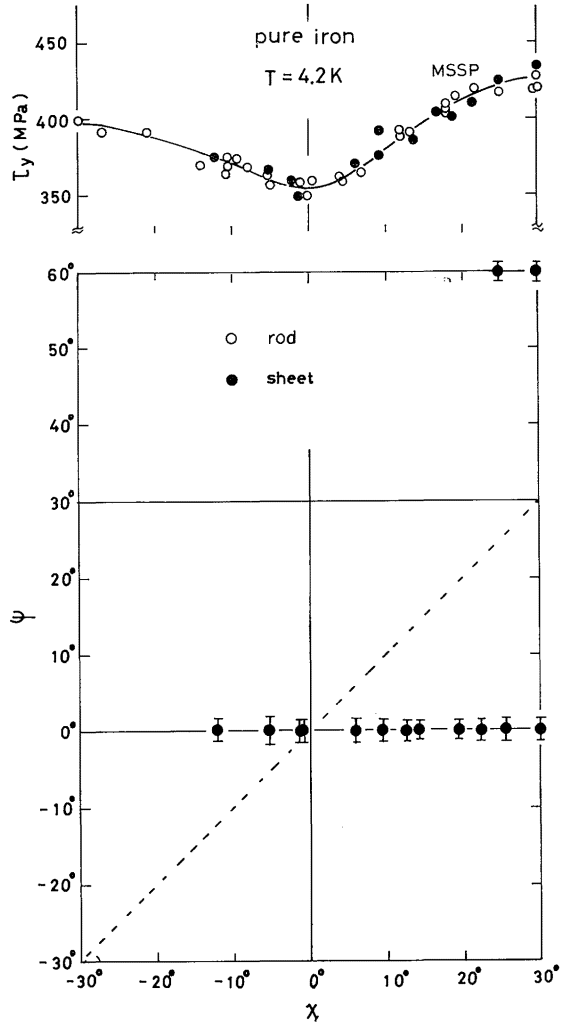

Fig. 40 τ_y—χ aßd ϕ—χ relations for pure iron at 4.2 K.

pile-up. It was made clear from the present experiment that the micro-twins was nucleated at a low stress level before macro-yielding at 4.2 K when the dislocation structure containing mixed dislocation is formed in a specimen by a small pre-strain at room temperature. From this fact it can be presumed that the nuleus of a twin is formed by the pile-up of non-screw dislocations. If such a nuleus is generated as a result of inhomogenous deformation, the probability of forming pile-up dislocations will be less in the specimen of a smaller size.

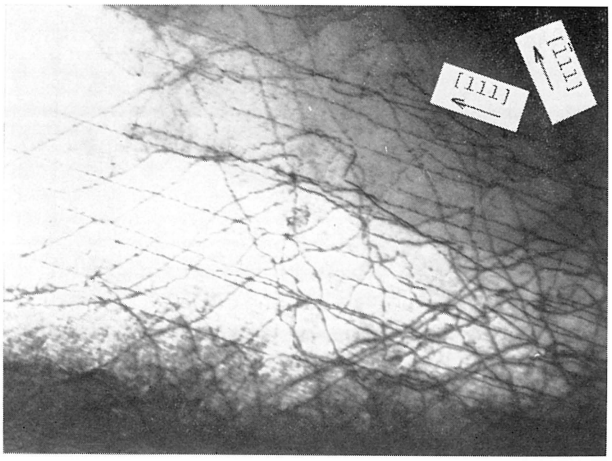

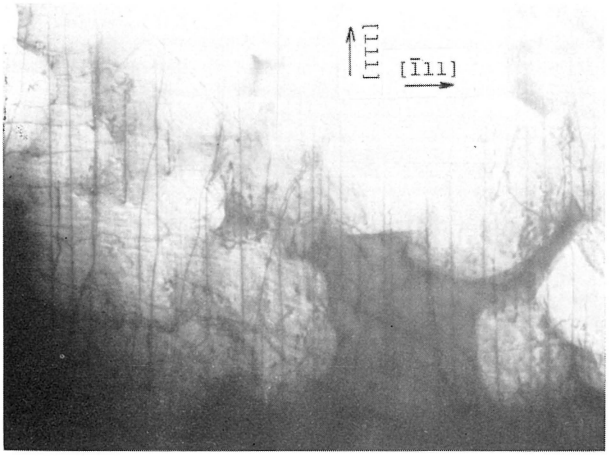

Fig. 41 Dislocation structure in the specimen of pure iron at 200 K (a) and 30 K (b) (2 % shear strain). ($\chi=4°$, $\lambda=46°$).

On the other hand, pole mechanism[61] has been offered as a mechanism of the growth of a twin. It is based on the interaction between a existing slip dislocation and a twin dislocation. The growth of a twin is assumed to be more suppressed in the specimens of smaller size if this mechanism is adopted since the number of pole dislocations is less

in the specimen of a smaller size. This suggestion is in good accord with the experimental result that the width of a twin is also smaller in the specimen of a small size (Fig. 21). The distance for twin propagating and the simultaneous growth to the width can be given by the maximum side of a specimen.

The deformation-mode at very low temperatures depending on the specimen size can be qualitatively explained by the mechanisms of the nucleation and growth of a twin mentioned above.

4.2. Mechanism of slip deformation in iron

Characteristic features of slip deformation in high-purity iron single crystals sufficiently free from the influence of impurity atoms were summarized:

(1) characteristic features of deformation divides the temperature range into three parts $T<150$ K, $150\text{ K}<T<340$ K and $T<340$ K.

(2) in the temperatue range $T<150$ K the yield stress shows strong temperature and orientation dependence when temperature is lowered. At 4.2 K the yield stress has a minimum at $\chi=0°$ and the orientation dependence of concave type with $\tau_y/\tau_{y,\chi=0°}=1.12$ and 1.22 at $\chi=-30°$ and 30°, respectively. This relation is invariant in the temperature range $T<150$ K.

(3) a hump appears on τ_y-T curve in the temperature range $150\text{ K}<T<300$ K. Activation area has a peak on $A^*-\tau_y$ curve in the same temperature range. These hump and peak disappear by the addition of solute carbon atoms.

(4) $\Delta H/kT$ gives a constant value of 26 in the temperature range above 30 K, but in the temperature range below 30 K it is reduced rapidly when temperature is lowered. The strain-rate sensitivity is constant below 10 K.

(5) the slip plane at 4.2 K is almost primary plane $(\bar{1}01)$ at any orientation. When temperature is elevated, the slip plane approaches the maximum shear stress plane on average from $(\bar{1}01)$. The dislocation structure is governed by the screw character below 200 K.

(6) in the temperature range $T>340$ K the temperature dependence of yield stress is weak and the orientation dependence disappears.

In this section, the experimental results mentioned above is discussed from a point of view of dislocation theory, particularly keeping in the accent on the BCC structure of iron.

It is clear that the strong temperature dependence of yield stress in (2) is generally based on Peierls mechanism (mechanism of lattice friction) of a screw dislocation in BCC metals. This is supported from dislocation structure in (5). As charcteristics of iron, the orientation dependence of yield stress in (2), the existence of a hump or peak in (3) and $(\bar{1}01)$ slip plane can be adopted. In comparison with other metals,

the similarities have been recently recognized, such as the orientation dependence of yield stress of concave type and $(\bar{1}01)$ slip plane at 4.2 K for Mo[76] and the existence of a hump in a lower temperature range for Mo[77] and Nb[78]. However, great difference between iron and other metals is the appearance of anomalous slip in the latter. The yield stress in the latter, therefore, generally shows the monotonous function of χ at all temperatures except Mo at 4.2 K[76]. The slip plane has been reported to be anomalous plane $(0\bar{1}\bar{1})$ in Mo[79], V[80] and Nb[81] in comparison with normal plane $(\bar{1}01)$ in iron and twinning plane $(\bar{1}\bar{1}2)$ in less pure Ta[29]. The difference in slip between BCC metals will have to be explained from the nature of the core structure of a screw dislocation based on the difference in inter-atomic force.

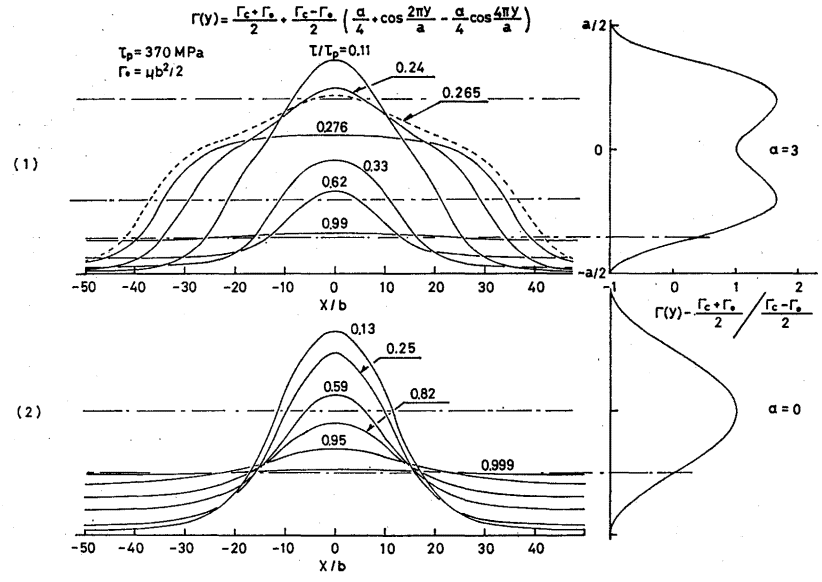

Fig. 42 Critical shape (saddle-point configuration) of the double kink on the Peierls potentials (camel-hump type ($\alpha=3$) and sinusoidal type ($\alpha=0$)) under various stresses. The direction of a screw dislocation is parallel to X axis. $\Gamma(y)$ is the line energy per unit length, Γ_c and Γ_0 the energy at the top and bottom of the Peierls potential, respectively and τ_p the Peierls stress.

The existence of a hump on τ_y-T curve, which corresponds to a peak on $A^*-\tau_y$ curve, can be explained from the Peierls potential of camel-hump type according to the semi-quantitative theory by Dorn et al.[82,83]. In Fig. 42, the calculated saddle-point configurations under each stress are shown for two cases of potentials of camel-hump type ($\alpha=3$) and usual sinusoidal type ($\alpha=0°$) where a screw dislocation is forming a

double kink on a potential by the aid of thermal fluctuation. Activation area is given by the area surrounded with the stable configuration of a screw dislocaion before forming a double kink and the saddle-point configuration. In case of camel-hump type, activation area has a peak at a stress level of $\tau/\tau_p=0.265$, which is indicated by broken line in the figure. In an alternative case, it monotonusly decreases with increasing stress. Thus, the existence of a hump and a corresponding peak in iron can be explained by the model of Peierls potential of camel-hump type.

However, it is not self-evident whether Peierls potential is essentially of camel-hump type or not, but Takeuchi et al.[21)84)85)] and Kuramoto et al.[86)], who have performed computer simulation for a screw dislocation using empirical interatomic row potentials, have given the interest results. Fig. 43 shows the typical core structures of a screw dislocation in a BCC crystal under zero stress. The core structures are roughly divided into two cases depending on the inter-atomic row potentials: degenerate type (with two equivalent configurations in energy) (a) and non-degenerate (close to the linear elasticity solution) (b). The former has been also reported by Vitek et al.[20)], who has used empirical inter-atomic potentials of Johnson. The latter also takes with metastable split configuration (c) at a half of the unit distance in the motion of a screw dislocation. This, therefore, means that Peierls potentials is of camel-hump type shown in (d). The case of (a) is of sinusoidal type.

When the core structure of a screw dislocation is of special non-degenerate type, the slip plane is almost normal $(\bar{1}01)$ plane from the results by Takeuchi et al.[24)84)85)]. This is in accord with the experimental result at 4.2 K. Such a non-degenerate core also gives almost the same $\tau_y-\chi$ relation of asymmetric concave type as that obtained from the present experiment. However, the value of calculated Peierls stress is higher by one order than the yield stress extrapolated to absolute zero temperature.

Very recently, Masuda and Sato[87)88)] have introduced the effect of d-electrons on the inter-atomic potential for simulating the core structure and the motion of a screw dislocation, instead of empirical potentials. Their results for iron show the same non-degenerate core and are in rather better accord with the present experimental results than those by Takeuchi, concept a slip plane.

According to theories by Dorn et al., Takeuchi et al. and Masuda and Sato mentioned above, the characteristic features of slip deformation in iron obtained in the present experiment can be explained from the motion of a screw dislocation with the non-degenerate core structure.

4.3. Quantum effect on a dislocation motion at very low temperatures

It was shown from the activation analysis that activation enthalpy or $\Delta H/kT$ rapidly decreases when temprature is lowered in (4). The same phenomenon has been observed in Ta[89)] in a BCC metal and ionic crys-

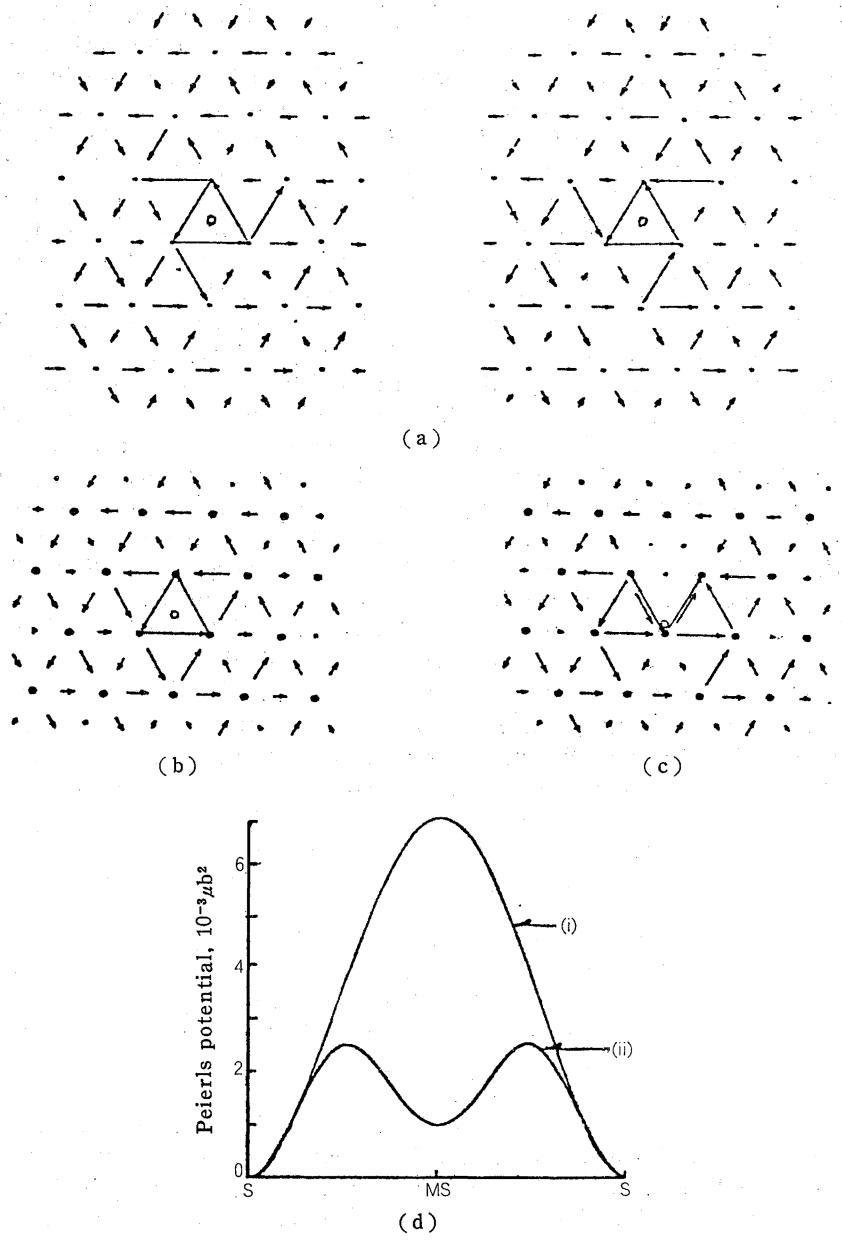

Fig. 43 Typical core structure of a screw dislocation viewed along Burgers vector under no stress for various inter-atomic row potentials reported by Takeuchi et al.: (a) degenerate core, (b) non-degenerate core and (c) metastable core, and Peierls potentials (i) and (ii) in (d) corresponding the cores (a) and (c), respectively.

tals[90], which are controlled by Peieris mechanism. This seemed to be a rather universal effect on thermally activated process at very low temperatures. The decrease of this exponent, $\Delta H/kT$ is too large to be explained by the change of the pre-exponential factors in the rate equation such as mobile dislocation density or the unit slip area in an activation event. It must be concluded then that some modifications are needed to the classical Arrhenius type rate equation in the low temperature region. As mentioned in the introduction two possibilities must be taken into account in the case of b.c.c. metals, i.e. (1) the effect of tunnelling of the dislocation through the potential barrier and (2) the quantum effect on the vibrational mode of the dislocation caused by discrete energy levels and the zero-point vibration. As for the first one, Arko and Weertman[91] and Natsik et al.[38] estimated the temperature below which the tunnelling effect becomes dominant and found it to be less than 1 K, although some ambiguities in the expression for the dislocation mass are contained. The fact that the deviation of the value of $\Delta H_{exp}/kT$ from the high-temperature constant value starts at around 30 K, as shown in Fig. 5, seems to show that the tunnelling effect is not responsible for this anomaly at low temperatures.

As for the second effect, details were already described by Takeuchi and Maeda[89] in a previous paper and here a brief review will be given below. The rate of the formation of a double kink is determined by the probability that the amplitude of the dislocation vibration exceeds a certain value at the saddle point configuration. Following the result of Alefeld[36], the probability is expressed by a form of the Arrhenius equation, $\dot{\gamma}=\dot{\gamma}_0 \exp(-\Delta H/kT)$, but with an effective temperature T_e, instead of T, given by

$$T_e = (\sum_i \alpha_i^2 \varepsilon_i)/(k \sum_i \alpha_i) \ , \tag{1}$$

with

$$\alpha_i = \sqrt{2}\ Q_i/\sqrt{M_i \omega_i}$$

and

$$\varepsilon_i = \frac{\hbar\omega_i}{2} \coth \frac{\hbar\omega_i}{2kT} \ .$$

Here, ε_i, ω_i, M_i and Q_i are average energy, angular frequency, effetive mass and the normalized eigenvector of ith mode of vibration, respectively. With the assumption of a narrow distribution of $\omega_i s$ that contribute to the double-kink nucleation, eq.(1) is approximated by

$$T_e \simeq \frac{T_0}{2} \coth \frac{T_0}{2T} \ , \tag{2}$$

with $T_0=\hbar\omega_0/k$, where ω_0 is a representative value of the frequency. T_e tends to $T_0/2$ at very low temperatures and to T at high temperatures.

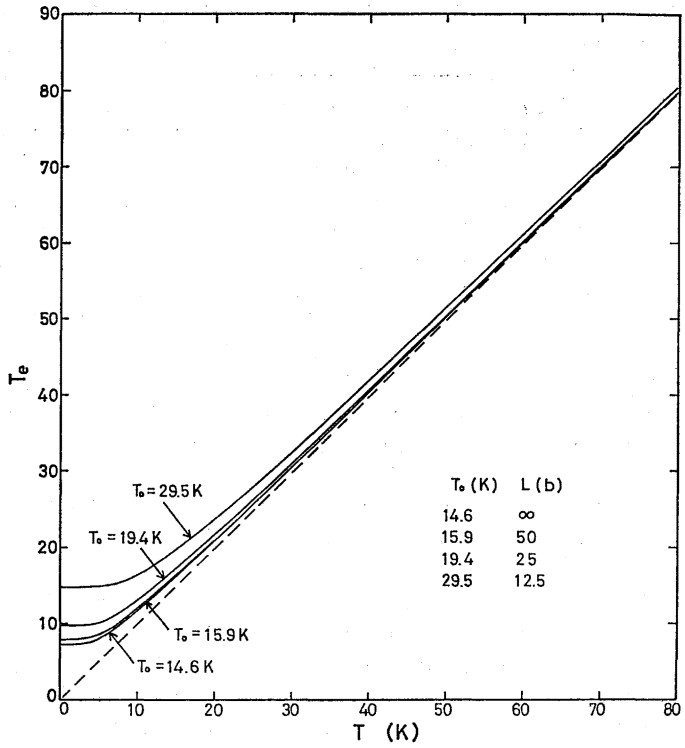

Fig. 44 Relation between T_e and T as a function of T_0.

The relation between T_e and T is shown in Fig. 44. Thus, the deformation of a crystal behaves quite differently from the classical rate equation for temperature below T_0. In particular, at zero temperature the activation enthalpy determined by eq.(2) has a non-vanishing value corresponding to the temperature $T_0/2$, which also suggests non-zero strain-rate sensitivity at zero degree, as seen in Fig. 30. Neglecting a weak dependence of the pre-exponential factor on temperature (Alefeld[36]), the experimental activation enthalpy found by the conventional process is written as

$$\Delta H_{\text{exp}} = \partial \ln \dot{\gamma} / \partial(-1/kT)\, \Delta H (T/T_e)^2 \partial T_e/\partial T \tag{3}$$

$(T/T_e)^2 \partial T_e/\partial T$ in eq. (3) is plotted against T in Fig. 45. For the constant strain-rate test, $\Delta H/kT_e$=constant$\equiv m$. Then, from eqs. (2) and (3).

$$\Delta H_{\text{exp}}/kT = m(T/T_e)\partial T_e/\partial T \simeq m(T_0/T)\ \text{cosech}\ (T_0/T) \tag{4}$$

The frequency of the dislocation segment with a length L vibrating in a Peierls potential valley is given approximately by (Leibfried[35])

$$\omega = v_s[(\pi/L)^2 + \tau^0/E]^{1/2} \tag{5}$$

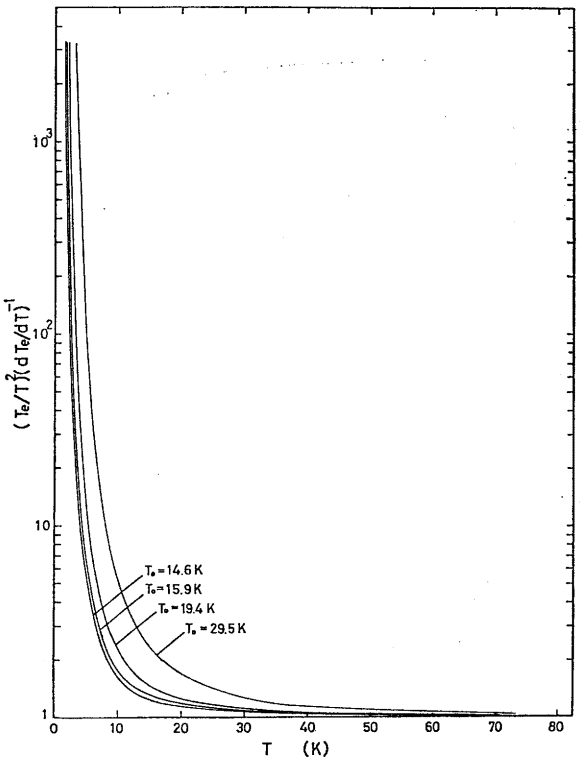

Fig. 45 Relation between $(T_e/T)^2(\partial T_e/\partial T)^{-1}$ and T as a function of T_0.

where v_s is the shear wave velocity, E the line energy of the dislocation and $\tau_0 b$ corresponds to the force constant of the Peierls potential valleg. Approximating the Peierls potential by two parabolic curves, one for the valley and the other for the hill, τ_0 is related to the Peierls stress τ_p by $\tau_0 = 4\tau_p$. The segment length L that contributes to the double-kink nucleation is related to the activation area A^* by $L \simeq A^*/d$, where d is the activation distance of the Peierls potential under stress. For the deformation around helium temperature, d will be of the order of 0.1 b. As in the case of the activation enthalpy, the relation between A^*_{exp} and A^* can be written as

$$A^*_{exp} = A^*(T/T_e) \simeq A^*(2T/T_e) \tanh \frac{T_0}{2T} \qquad (6)$$

The relation between T_e/T and T is shown in Fig. 46. Values of A^* have been calculated, as shown in Fig. 47. At helium temperature the value of A^* is about $5\,b^2$, which gives about 50 b for the value of L as a representative value in the present temperature range. Hence, values

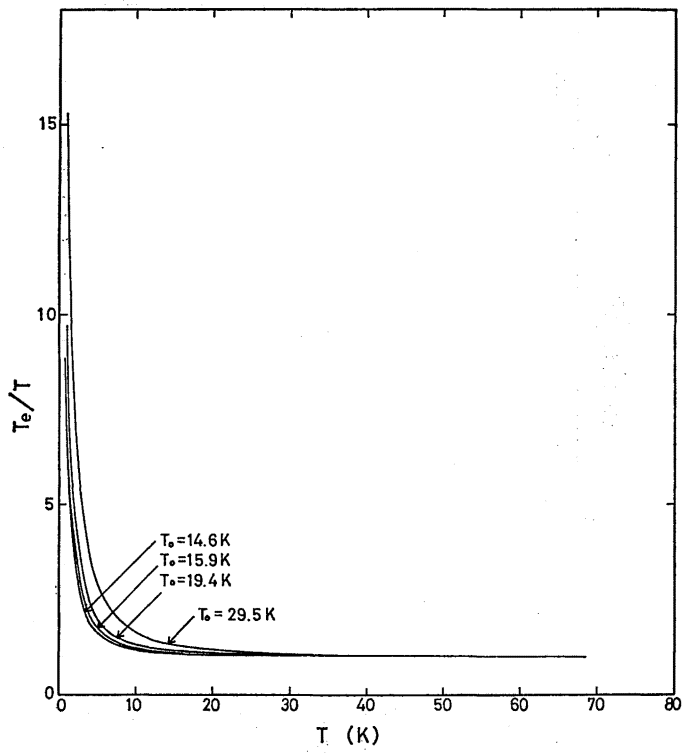

Fig. 46 Relation between T_e/T and T as a function of T_e.

of T_0 have been estimated to be 15 and 16 K for orientations A and B, respectively, using $v_s=3.3\times10^3$m/s, $\tau_p=370$ MN/m^2 (orientation A) and 450 MN/m^2 (orientation B) and $E\simeq\mu b^2=5.3\times10^{-9}$ J/m. In Fig. 48 the relation between $\Delta H_{exp}/kT$, normalized by the asymptotic value of $m(\sim26)$ and the reduced temperature T/T_0 (eq.(4)), is shown by a solid line together with experimental values. The agreement between the theory and experiment is satisfactory taking account of the above many simplifications of the argument.

In conclusion, therefore, a remarkable deviation from the Arrhenius rate equation below 30 K observed in the deformation of high-purity iron single crystals can reasonably be interpreted by the quantum effect of the dislocation vibration in overcoming the Peierls potential.

Very recently, the comment to our insistence based on theory of Alefeld have been made by H. Suzuki[91]. His insistence is that the zero-point energy is the lowest energy, is not allowed to cause any fluctuation of vibrational energy in a fractional part of a vibrating system and therefore effective temperature is not represented by the sum of the

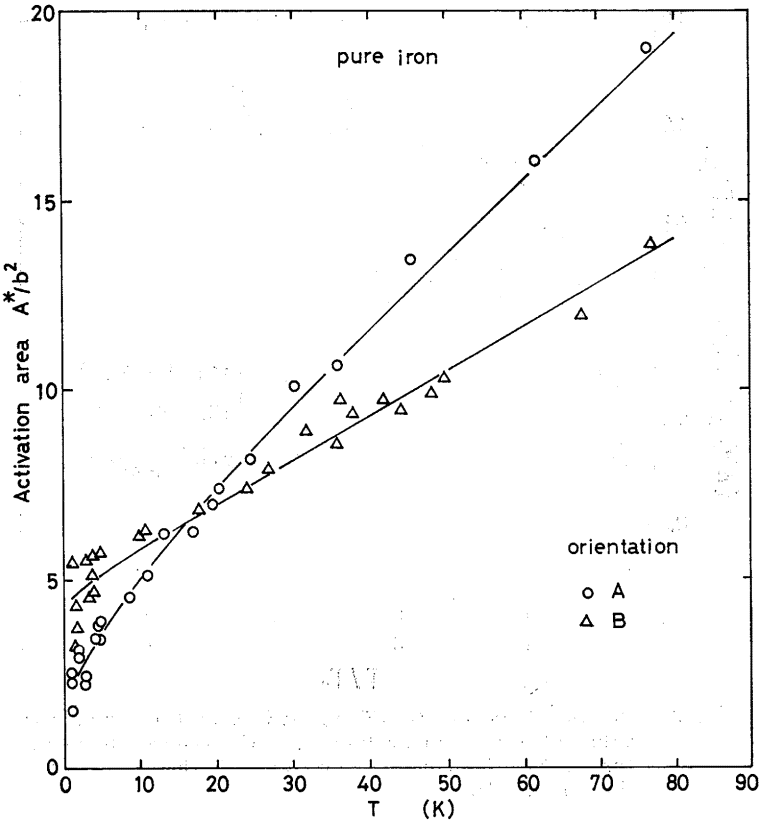

Fig. 47 Temperature dependence of the true activation area calculated according to eq. (6).

zero-point energy and the thermal energy. He has suggested the opinion of the process of emission of a double kink absorbing a phonon from the analogy of the photo-electric excitation.

Acknowlegements

The authors wish to thanks Mr. H. Abe for his help in the experiment and his useful discussion on the experimental results. They are also gratefull to Messrs Y. Miyamoto and T. Fujiwara for the production of high-purity iron single crystals and their help in the experiment.

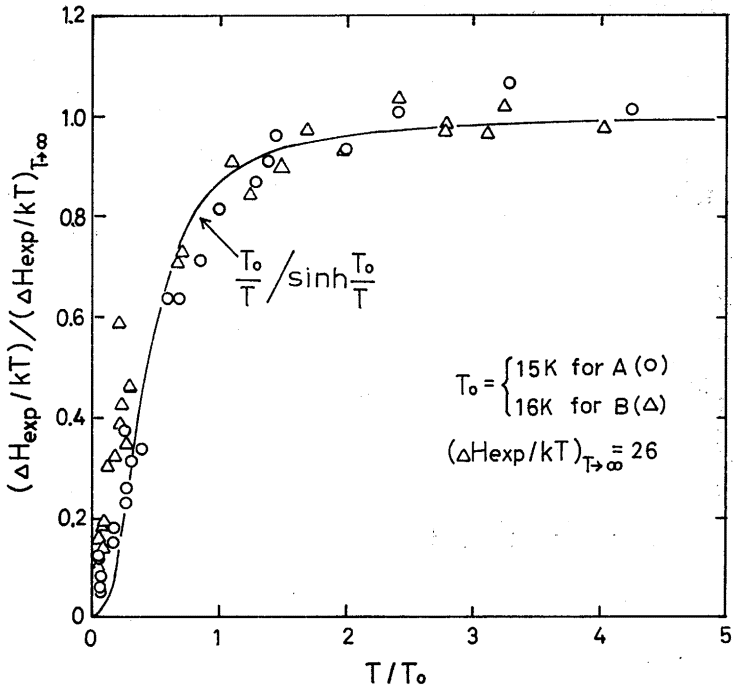

Fig. 48 Relation between $\Delta H/kT$ normalized by the asymptotic value at high temperatures and the reduced temperature T/T_0. Solid curve represents thetheoretical relation of eq. (4).

References

1) Allen, N. P., Hopkins, B. E. and McLennan, L. E.: Proc. Roy. Soc. **A 234** (1956) 221.
2) Conte, R., Groh, P. and Escaig, B.: Phys. Stat. Sol. **28** (1968) 475.
3) Meshii, M. and Sato, A.: Proc. Int. Conf. on Fundamental Aspects of Radiation Damage in Metals, Gatlinburg, Tennessaa, USA (1975) 984.
4) Matsui, H., Moriya, S., Takagi, S. and Kimura, H.: Trans. JIM **19** (1978) 163.
5) Basinski, Z. S. and Christian, J. W.: Austr. J. Phys. **13** (1960) 299.
6) Conrad, H. and Schoeck, G.: Acta Met. **8** (1960) 791.
7) Conrad, H.: Phil. Mag. **5** (1960) 745.
8) Conrad, H. and Frederik, S.: Acta Met. **10** (1962) 1013.
9) Conrad, H.: *Iron and its Dilute Solid Solution*, Interscience (1963) 315.
10) Stein, D. T., Low Jr., J. R. and Seybolt, A. U.: Acta Met. **11** (1963) 1253.
11) Stein, D. F. and Low Jr., J. R.: Acta Met. **14** (1966) 1183.
12) Arsenault, R. J.: Acta Met. **12** (1964) 547.
13) Alshuler, T. L. and Christian, J. W.: Phil. Trans. Roy. Soc. **261** (1967) 253.
14) Keh, A. S. and Nakada, Y.: Canad. J. Phys. **45** (1967) 1101.

15) Spitzig, W. A. and Keh, A. S.: Acta Met. **18** (1970) 1021.
16) Spitzig, W. A.: Acta Met. **18** (1970) 1275.
17) Fleischer, R. L.: Acta Met. **15** (1967) 1513.
18) Hirsch, P. B.: Proc. 5th Int. Congress of Crystallography, Cambridge, (1960) 139; *Dislocation Dynamics*, McGraw-Hill, New York (1968) 57.
19) Suzuki, H.: *Dislocation Dynamics*, McGraw-Hill, New York (1968) 679.
20) Vitek, V.: Crystal Lattice Defects 5 (1974) 1; Phil Mag. **21** (1970) 1049; Phil Mag. **21** (1970) 1275.
21) Minami, F., Kuramoto, E. and Takeuchi, S.: Phys. Stat. Sol. (**a**)**12** (1972) 581.
22) Minami, F., Kuramoto, E. and Takeuchi, S.: Phys. Stat. Sol. (**a**) **22** (1974) 81.
23) Kuramoto, E., Minami, F. and Takeuchi, S.: Phys. Stat. Sol. (**a**) **22** (1974) 441.
24) Takeuchi, S. and Kuramoto, E.: J. Phys. Soc. Japan **38** (1975) 480.
25) Takeuchi, S.: Phil. Mag. **39** (1979) 661.
26) Spitzig, W. A. and Keh, A. S.: Met. Trans. **1** (1970) 2751.
27) Lau, S. S. and Dorn, J. E.: Phys. Stat. Sol. (**a**) **2** (1970) 825.
28) Argon, A. S. and Maloof, S. R.: Acta Met. **14** (1966) 1449.
29) Takeuchi, S., Kuramoto, E. and Suzuki, T.: Acta Met. **20** (1972) 909.
30) Taoka, T., Takeuchi, S. and Furubayashi, E.: J. Phys. Soc. Japan **19** (1964) 701.
31) Mott, N. F.: Phil. Mag. **1** (1956) 568.
32) Weertman, J.: J. Appl. Phys. **29** (1958) 1685.
33) Gilman, J. J.: J. Appl. Phys. **39** (1968) 6086.
34) Petukhov, B. V. and Pokr vskii, V. L.: Soviet Phys. JETP **36** (1973) 336.
35) Leibfried, G.: *Dislocation and Mechanical Properties of Crystals*, New York, John Wiley (1957) 495.
36) Alefeld, G.: Phys. Rev. Lett. **12** (1964) 372.
37) Suzuki, H.: Fundamental Aspects of Dislocation Theory, U. S. National Bureau Standards (1970) 317.
38) Nastik, V. D., Osetskii, A. I., Soldatov, V. P. and Startsev, V. I.: Phys. Sol. (**b**) **54** (1972) 99.
39) Suzuki, T. and Ishii, T.: *Physics of Strength and Plasticity*, M. I. T. Press (1969) 159.
40) Suenaga, M. and Galligan, J. M.: *Physical Acoustics*, Vol. 9, Academic Press (1972) 1.
41) Granato, A. V.: *Internal Friction and Ultrasonic Attenuation in Solids*, Univ. of Tokyo Press (1977) 81.
42) Takagi, S. and Kimura, H.: Scripta Met. **10** (1976) 701.
43) Takagi, S. and Kimura, H.: Scripta Met. **10** (1976) 1095.
44) Kitajima, K.: Private communication.
45) Wagenblast, H. and Arajs, S.: J. Appl. Phys. **39** (1968) 5885.
46) Sato, A. and Meshii, M.: Scripta Met. **8** (1976) 851.
47) Kuramoto, E.: Thesis, Univ. of Tokyo.
48) Spitzig, W. A. and Keh, A. S.: Acta Met. **18** (1970) 11.
49) Mitchell, T. E., Foxall, R. A. and Hirsch, P. B.: Phil. Mag. **8** (1963) 1895.
50) Tomalin, D. S. and Stein, D. F.: Trans. Met. Soc. AIME **233** (1965) 2066.
51) Quesnel, D. J., Sato, A. and Meshii, M.: Mater. Sci. Eng. **18** (1975) 199.
52) Diel, J., Schreiner, M., Staiger, S. and Zwiesele, S.: Scripta Met. **10** (1976) 949.
53) Tseng, D. and Tangri, K.: Scripta Met. **11** (1977) 719.
54) Tangri, K. and Loyd, D. J.: Scripta Met. **7** (1973) 915.
55) Nakada, Y. and Keh, A. S.: Acta Met. **16** (1968) 903.

56) Okazaki, K., Kagawa, M. and Aono, Y.: Z. Metallkde **67** (1976) 47.
57) Cottu, J. P., Reyrade, J. P., Chomel, P. and Groh, P.: Acta Met. **26** (1978) 1179.
58) Matsui, M., Kimura, A. and Kimura, H.: Proc. 5th Int. Conf. on the Strength of Metals and Alloys, Aachen, W. Germany (1979) 977.
59) Ikeda, S.: J. Phys. Soc. Japan **27** (1969) 1564.
60) Nagakawa, J., Sato, A. and Meshii, M.: Phil. Mag. **31** (1975) 1107.
61) Cottrell, A. H. and Bilby, B. A.: Phil. Mag. **42** (1951) 573.
62) Thompson, N. Milland, D. T.: Phil. Mag. **43** (1952) 442.
63) Sleeswyk, A. W.: Phil. Mag. **8** (1963) 1467.
64) Ogawa, K.: Phil. Mag. **11** (1965) 217.
65) Priestner, P. and Leslie, W. C.: Phil. Mag. **11** (1965) 895.
66) Orowan, E.: *Dislocation in Metals*, New York (1954) 116.
67) Votava, E., Sleeswyk, A. W.: Acta Met. **10** (1962) 965.
68) Ogawa, K. and Maddin, R.: Acta Met. **12** (1964) 713.
69) Mahajan, S.: Acta Met. **23** (1975) 671.
70) Mahajan, S.: Phil. Mag. **A 26** (1972) 161.
71) Mahajan, S.: J. Phys. **F 2** (1972) 19.
72) Levonmaa, R. J. and Lindroos, V. K.: Scan. J. Metallur. **6** (1977) 92.
73) Ogawa, K. and Takeuchi, T.: Proc. Electron Microscopy Society of America, 29th annual meeting, Claitor's publishing division, Baton Rouge, La. (1971) 104.
74) Vitek, V.: Proc. 2nd Int. Conf. on the Strength of Metals and Alloys (1972) 389.
75) Yamaguchi, M. and Vitek, V.: Phil. Mag. **34** (1978) 1.
76) Keh, A. S., Spitzig, W. A. and Nakada, Y.: Phil. Mag. **23** (1971)
76) Kitajima, D., Aono, Y. and Kuramoto, E.: Scripta Met., to be published.
77) Aono, Y., Kuranoto, E. and Kitajima, K.: Acta Met., to be published.
78) Statham, C. D., Koss, D. A. and Christian, J. W.: Phil. Mag. **26** (1972) 1089.
79) Matsui, H. and Kimura, H.: Mater. Sci. Eng. **21** (1976) 247.
80) Taylor, G., Rajaj, R. and Carlson, O. N.: Phil. Mag. **28** (1973) 1035.
81) Garratt-Reed, A. J. and Taylor, G.: Phil. Mag. **33** (1979) 597.
82) Dorn, J. E. and Rajnak, S.: Trans. AIME **230** (1964) 1052.
83) Guyot, P. and Dorn, J. E.: Canadian J. Phys. **45** (1967) 983.
84) Takeuchi, S.: Phil. Mag. **A 39** (1979) 661.
85) Takeuchi, S.: in press (from ASM).
86) Kuramoto, E., Aono, Y. and Tsutsumi, T.: Rep. Res. Inst. Appl. Mech. **28** (1981) 91.
87) Masuda, D. and Sato, A.: Phil. Mag. **37** (1978) 531.
88) Sato, A. and Masuda, K.: Phil. Mag. **43** (1981) 1.
89) Takeuchi, S. and Maeda, K.: Acta Met. **21** (1977) 1485.
90) Suzuki, Tak.: private communication (1977).
91) Suzuki, H.: in press (from AIME).
92) Orowan, E.: Proc. Phys. Soc. **52** (1940) 8.
93) Kocks, U. F., Argon, A. S. and Ashby, M. F.: Prog. Mater. Sci. vol. **19** (1975) p. 91.

(Received May 8, 1981)

Appendix

Definition of activation parameters

The average velocity, $\bar{v}$ of a dislocation that surmounts obstacles with the assistance of thermal fluctuations is assumed to be given by a Arrhenius type relationship:

$$\bar{v} = A\upsilon \exp\left(-\frac{\Delta G(\tau^*, T)}{kT}\right) \tag{A1}$$

where A is the distance moved after a successful fluctuation, υ the frequency of vibration of the dislocation, $\Delta G(\tau^*, T)$ the Gibbs free energy of activation, k Boltzmann's constant and T temperature. This equation only applies when there are no back-fluctuation. The plastic strain-rate is also related the velocity of mobile dislocation through the Orowan equation[92]:

$$\dot{\gamma} = \rho_m b\bar{v} \tag{A2}$$

where ρ_m is the density of mobile dislocation and b is Burgers vector.

The combination of eqs. (A 1) and (A 2) yields a typical Arrhenius rate equation of deformation:

$$\dot{\gamma} = \dot{\gamma}_0 \exp\left(-\frac{\Delta H}{kT}\right) \tag{A3}$$

from $\Delta G = \Delta H - \Delta S$

where $\dot{\gamma}_0$ is $A\upsilon\rho_m b \exp(\Delta S/k)$ and ΔH and ΔS is activation enthalpy and entropy, respectively. Based on eq. (A 3) and the assumption of constant ΔS, the activation enthalpy may be expressed as

$$\Delta H = -kT^2 \exp\left(\frac{\partial \ln \frac{\dot{\gamma}}{\dot{\gamma}_0}}{\partial \tau^*}\right)_T \left(\frac{\partial \tau^*}{\partial T}\right)_{\dot{\gamma}} = -bA^*T\left(\frac{\partial \tau^*}{\partial T}\right)_{\dot{\gamma}} \tag{A4}$$

and the activation area is defined as

$$A^* = -\frac{kT}{b}\frac{1}{\beta}\bigg|_T \tag{A5}$$

where β is strain-rate sensitivity and is given by

$$\beta = \left(\frac{\partial \tau^*}{\partial \ln \frac{\dot{\gamma}}{\dot{\gamma}_0}}\right)_T \tag{A6}$$

Activation area and strain-rate sensitivity can be determined from stress relaxation test using fundamental equations mentioned above.

The imposed strain-rate during a constant strain-rate can be divided into two components, elastic and plastic:

$$\dot{\gamma}_t = \dot{\gamma}_e + \dot{\gamma}_p \tag{A7}$$

when the crosshead is stopped for the load to be relaxed, $\dot{\gamma}_t = 0°$ and

$$\dot{\gamma}_p = -\dot{\gamma}_e = -K_m\dot{\tau} \tag{A8}$$

where $K_m = 1/E + A_0/Sl_0$, A_0 and l_0 are the guage area and length of a specimen at the beginning of relaxation, respectively, and $\dot{\tau}$ the stress-rate during stress relaxation. S and E are the spring constant and Young's modulus, respectively. Strain-rate sensitivity of eq. (A 6) is, therefore, rewritten to the form:

$$\beta = \left.\frac{\partial\tau^*}{\partial \ln\left(-\frac{\dot{\tau}}{M}\right)}\right|_T$$

or

$$\frac{1}{\beta} = \left.\frac{\partial \ln(-\dot{\tau})}{\partial\tau^*}\right|_T - \left.\frac{\partial \ln M}{\partial\tau^*}\right|_T \tag{A9}$$

by use of eq. (A 8), where M is γ_0/K_m.

During stress relaxation eq. (A 9) is given as a function of relaxation time, t. The physical quantities obtained from the stress relaxation curve are the relaxed stress, $\Delta\tau_R(t)$ and stress-rate, $-\dot{\tau}(t)$. From the plots of $\Delta\tau_R$ and $-\dot{\tau}$, the slope, $-\partial \ln(-\dot{\tau})/\partial\Delta\tau_R$ is obtained. This slope is equivalent to $\partial \ln(-\dot{\tau})/\partial\tau$ from the relation of $\Delta\tau_R = \tau_0 - \tau$, where τ_0 is the applied stress at the beginning of relaxation. As stress relaxation advancing, the athermal stress component, τ_μ and the pre-exponential factor, M, especialy the density of mobile dislocation, ρ_m in it, will change gradually. The true strain-rate sensitivity which corresponds to the flow stress at the beginning of stress relaxation must be then estimated by taking account of these changes. This can be done by extrapolating back to $t=0$, where the additional changes appraoch zero value. Namely, one has

$$\lim_{t\to 0}[\partial \ln(-\dot{\tau})/\partial\tau] = \lim_{\delta\tau_\mu\to 0}[\partial \ln(-\dot{\tau})/\partial\tau] = \partial\ln(-\dot{\tau})/\partial\tau\Big|_{\text{or } \substack{-\tau=-\tau_0\\ \tau=\tau_0}} \tag{A10}$$

and

$$\lim_{t\to 0}[\partial \ln M/\partial\tau] = \lim_{\substack{\delta M\to 0\\ \text{or } \delta\rho_m\to 0}} \lim_{\delta\tau_\mu\to 0}[\partial \ln M/\partial\tau] = 0 \tag{A11}$$

Therefore, the true strain-rate sensitivity and activation area are obtained from the curve of $\ln(-\dot{\tau})$ v.s. $\Delta\tau_R$ as follows:

$$\beta = 1/[\partial \ln(-\dot{\tau})/\partial(\Delta\tau_R)]\,|_{\Delta\tau_R=0} \qquad \text{(A12)}$$

$$A^* = -\frac{kT}{b}[\partial \ln(-\dot{\tau})/\partial(\Delta\tau_R)]\,|_{\Delta\tau_R=0} \qquad \text{(A13)}$$

In general one can think that a decrease in stress in a time interval short compared to $y_m/\bar{v}$ cannot change ρ_m, where y_m is a mean free path[93].

Activation enthalpy can be obtained from eq. (A 13) and the slope, $\left(\frac{\partial\tau_y}{\partial T}\right)_{\dot{\tau}}$ under the assumption that temperature dependence of τ_μ is negligible.